Part II
Special Topics

Chapter 6

Carrier Phase Measurements and Cycle Slips

Carrier phase measurements represent an evolution with respect to code phase measurements described in the first part of the thesis. They are in principle able to provide centimetre level accuracy, but there are important hurdles that actually prevent their use in commercial and mass-market devices. First, carrier measures are affected by ambiguity related to the RF signal wavelength, which has to be solved to compute a PVT solution, with a non-trivial and computational demanding process. Then the issue of cycle slips has to be faced.

This chapter first outlines the principle and the benefits of carrier phase positioning (Section 6.1). Then clarifies the reasons why they are not likely to be implemented in single frequency mass-market receivers.

Nevertheless, it is expected that in the incoming years, thanks to the improvements in electronics, to the availability of faster, cheaper and smaller processors, and to the enhancements obtained by the research in this field, carrier phase measurements can start to be considered also in this category of receivers.

6.1 The principle of carrier phase positioning

GNSS carrier phase positioning techniques, based on the computation of the phase difference between the local carrier and the carrier of the received signal, are able to provide more accurate range measurements with respect to standard code measurements [4]. However several problems are present: first, carrier phase measurements are *ambiguous*. They contain an unknown number of carrier cycles, usually denoted *integer ambiguity*. This value remains constant during the signal tracking, as long as no cycle slips occur, and must be estimated by the receiver (integer ambiguity resolution) in order to compute correct measures. Second, the issue of cycle slips has to be faced; if a cycle slip occurs, the value of the ambiguity changes and the PLL shifts to a different stability point without taking notice.

Usually, carrier phase positioning and consequently cycle slip detection and mitigation are adopted only in dual frequency professional receivers, mainly for geodetic or monitoring purposes. Nevertheless, it is interesting to analyse the potentialities offered by these algorithms also for standard single frequency receivers, with a particular focus on SDR receivers.

6.1.1 Signal and system model

The GNSS signal model has been presented in Chapter 2. What is more, when dealing with carrier phase measurements, it necessary to introduce the dependency of the Doppler frequency with time. The expression of the signal after the signal conditioning, as reported in (3.2), can then be rewritten as

$$r[n] = \sqrt{2C}d(nT_s - \tau)c(nT_s - \tau)\bar{c}(nT_s - \tau)\cos\left[2\pi(f_{IF} + f_D(nT_s))nT_s + \varphi\right] + \eta_{IF}(nT_s)\,. \quad (6.1)$$

The difference between initial phase and instantaneous phase

First, it is important to underline a terminology problem, arising any time sinusoidal signals are concerned. The expression of the received GNSS signal reported in (2.3) can be expressed more generally as:

$$r(t) = A\cos\psi(t) + \eta_{RF}(t)\,, \quad (6.2)$$

where

$$\psi(t) = 2\pi\left(f_{RF} + f_D(t)\right)t + \varphi_0\,. \quad (6.3)$$

In (6.2), two different phase components can be identified:

- the argument of the sinusoid, $\psi(t)$, is called **instantaneous phase** of the signal and is time varying;
- the term φ_0 is called **initial phase** of the signal and it is constant. It represents just an initial shift, i.e. the instantaneous phase at time $t = 0$.

In the following, the term phase, when not specified, is used in the first meaning of time-varying instantaneous phase.

The concept of instantaneous frequency

When dealing with a sinusoidal signal as the one of (6.2), two cases can be distinguished.

1. The signal $r(t)$ is an ideal periodic sinusoid with period T_0. In this case $\psi(t)$ is a linear function of time t of the type
$$\psi(t) = 2\pi\frac{1}{T_0}t + \varphi_0\,, \quad (6.4)$$
where
$$f_0 = \frac{1}{T_0} \quad (6.5)$$
is a constant, equal to the multiplicative inverse of period and called **frequency**, and φ_0 is the initial phase. This assumption, normally made when performing code-based measurements, has been considered throughout the first part of the thesis.

2. The signal $r(t)$ is not a periodic sinusoid. In this case the frequency of the received signal cannot be considered constant, and the concept of frequency as inverse of the period should be abandoned. A different concept of frequency is introduced, which is the **instantaneous frequency** (reflecting its dependency on the time), defined as an instantaneous phase rate:
$$f_i(t) = \frac{1}{2\pi}\frac{d}{dt}\psi(t)\,. \quad (6.6)$$
The concept of instantaneous phase is kept. In addition, (6.6) coincides with (6.5) if $\psi(t)$ is linear.

The second case is more representative of real GNSS scenarios, in which the signal is not periodic, because, a part from noise, the reciprocal and continuous motion between the transmitter and the receiver induce a time varying Doppler effect. Recalling (6.3), the instantaneous frequency can be computed as

$$\begin{aligned} f_i(t) &= \frac{1}{2\pi}\frac{d}{dt}\psi(t) && (6.7)\\ &= \frac{1}{2\pi}\frac{d}{dt}2\pi\left(f_{RF} + f_D(t)\right)t + \varphi_0 \\ &= \frac{1}{2\pi}\left(\frac{d}{dt}2\pi f_{RF}t + \frac{d}{dt}2\pi f_D(t)t + \frac{d}{dt}\varphi_0\right) \\ &= f_{RF} + \frac{d}{dt}f_D(t)t && (6.8)\\ & && (6.9) \end{aligned}$$

The phase integer ambiguity

While code delay measurements are unambiguous, carrier phase measurements are **ambiguous**. Carrier phase is measured in terms of the number of cycles generated or received since a starting point. If, at a given time instant t_0, $\psi(t_0)$ can be written as

$$\psi(t_0) = 2\pi N(t_0) + \psi_{\text{frac}}(t_0)\,, \tag{6.10}$$

where $N(t_0)$ is an integer and $|\psi_{\text{frac}}(t_0)| < 2\pi$, then we have

$$r(t) = A\cos\psi(t_0) = A\cos\psi_{\text{frac}}(t_0)\,. \tag{6.11}$$

It is evident that, by inverting $r(t_0)$ with an arcosine operation, it is not possible to distinguish between $\psi(t_0)$ and $\psi_{\text{frac}}(t_0)$. Therefore, the integer part $N(t_0)$ cannot be recovered from $r(t_0)$. In other words, the phase measurement contain an unknown number of carrier cycles, denoted **integer ambiguity**. On the other hand, $\psi_{\text{frac}}(t_0)$, called **fractional phase**, can be recovered, provided that both $\cos\psi(t_0)$ and $\sin\psi(t_0)$ are available.

Figure 6.1 depicts this fact: when the receiver starts the tracking stage, at time t_0, a certain and unknown number $N(t_0)$ of carrier cycles affect the measurement. At times t_1, t_2, t_n, the receiver accumulates phase observations, respectively Φ_1, Φ_2, Φ_n. $N(t_0)$ remains constant during the tracking of the signal, as long as no cycle slips occur. Therefore, in order to compute correct ranges, it should be computed by the receiver, with a process denoted *integer ambiguity resolution* [78].

Instantaneous, initial, and fractional phases are three different phase terms, playing different roles in PLLs. When dealing with carrier phase measurements it is important to be aware of their differences.

Carrier phase pseudo-range

The carrier phase is the difference between the phase of the carrier of the received signal and the phase of the local carrier generated by the receiver, exploiting the information given by the PLL and the DLL. Carrier phase measurements represent an indirect and accurate measure of the range between receiver and satellite. It can indeed be proved that carrier phase measurements are more accurate than normal code delay based measurements, introduced in Section 2.6. For GPS L1 and Galileo E1 signals, the wavelength λ is equal to about 19 cm, and the carrier phase can be measured with a typical accuracy of $0.01 - 0.02$ cycles, with a resulting accuracy in the range $2\text{ mm} - 1\text{ cm}$ [78].

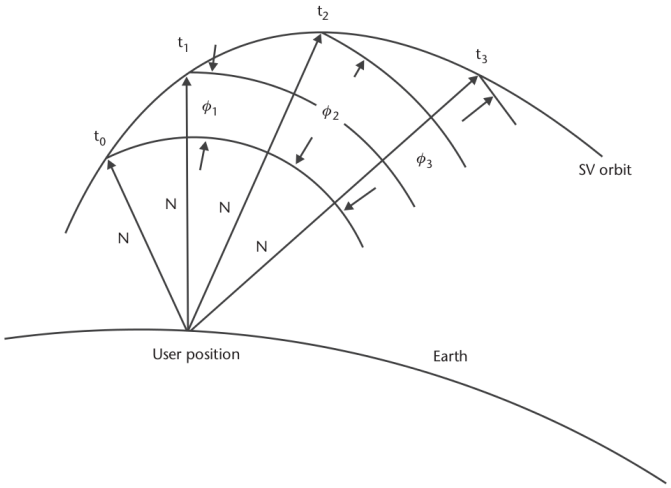

Figure 6.1: Carrier-phase ambiguity geometric relationships [17].

As done for the code measurements in the previous section, also for carrier measurements it is possible to relate the phase at the satellite at the time of transmission by the transit time of the signal. The carrier phase measurement in unit of cycles, $\phi(t)$, can be expressed as the difference between the instantaneous phase φ_u of the locally generated carrier and the instantaneous phase φ^s of the carrier of the received signal, plus the unknown number of cycles:

$$\phi(t) = \varphi_u(t) - \varphi^s(t-\tau) + N\,, \tag{6.12}$$

where

- $\varphi_u(t)$ is the instantaneous phase of the local carrier at time t;
- τ is the signal transmit time;
- $\varphi_s(t-\tau)$ is the instantaneous phase of the received signal at time t, corresponding to the phase of the transmitted signal at time $t-\tau$;
- N is the unknown number of cycles.

It can be proved, assuming a perfect synchronization, $\varphi_u(t) = \varphi^s(t)$, that:

$$\varphi_u(t) - \varphi^s(t-\tau(t)) = f\tau(t)\,, \tag{6.13}$$

where f_{RF} is the central carrier frequency of the SIS.

Therefore, combining (6.12) and (6.13), we have:

$$\begin{aligned} \phi(t) &= \varphi_u(t) - \varphi^s(t-\tau) + N = \\ &= f_{RF}\tau(t) + N \\ &= \frac{c}{\lambda}\frac{r(t,t-\tau)}{c} + N \\ &= \frac{r(t,t-\tau)}{\lambda} + N \end{aligned}\,, \tag{6.14}$$

where and $r(t, t-\tau)$, as before, is the geometric range between user position at time t and satellite position at time $t-\tau$. Finally, the apparent range between the transmitter and the receiver r at time t can be computed as:

$$r(t, t-\tau) = \lambda \left(N + \phi(t)\right) , \tag{6.15}$$

where N is the integer ambiguity to be estimated, whose sign is kept positive with respect to (6.14) without losing generality.

The fractional phase measurement, $\phi(t)$, is computed by the receiver at the conclusion of each epoch. It corresponds to the accumulation of the advances in carrier phase during an epoch. The advance in carrier phase is determined by integrating the carrier Doppler frequency offset update over the epoch; therefore the phase measurement is computed according to the following equation:

$$\phi(t) = \phi(t_0) + \int_{t_0}^{t} f_D(\tau)\, d\tau + \phi_r(t) . \tag{6.16}$$

That corresponds in the discrete time digital domain, to

$$\begin{cases} \phi[n] = \phi[n-1] + \sum_{k=n-1}^{n} f_D[k] + \phi_r[n] \\ \phi_r[n] = \mathrm{rem}\left(\theta_{RX}\left[n\right] - \theta_{loc}\left[n\right], 2\pi\right) \\ \phi[1] = A \end{cases} , \tag{6.17}$$

where:

- $\phi[n]$ is the accumulated phase at epoch n;
- f_D is the Doppler frequency;
- $\phi_r[n]$ is the fractional phase at epoch n;
- A is a whole plus fractional arbitrary cycle count.

In addition it can be proved that [4]

$$\sum_{k=n-1}^{n} f_D[k] = f_D[n] T_c , \tag{6.18}$$

where T_c is the integration period.

Finally the expression of the range between satellite and receiver is expressed as

$$r[n] = \lambda \left(N + \phi[n]\right) . \tag{6.19}$$

Once the integer ambiguity has been solved (in the navigation stage), the correct ranges can be computed.

Moreover, it has to pointed out that the model described above is valid only in absence of *cycle slips*. In fact, as described above, carrier phase continuity is of major importance for the measurement to be useful. If a signal lock occurs, a jump in the instantaneous accumulated phase is experienced and the value of N changes. It is then necessary to take into account this factor, to correct the value of N, in order to compute correct range values. For this reason it is necessary to better analyse the phenomenon of cycle slips.

As done for code measurements, in order to account for the clock biases, initial phase offsets, atmospheric propagation delays and measurements errors, a more complete expression is introduced. It is denoted carrier phase observation equation [22, 4]:

$$\phi(t) = \frac{r(t, t-\tau) - I_\phi(t) + T_\phi(t)}{\lambda} + \frac{c}{\lambda}\left(\delta t_u(t) - \delta t^s(t-\tau)\right) + N + \varepsilon_\phi(t) , \tag{6.20}$$

where ε_ϕ is a general noise term. (6.20) appears very similar to code phase observation equation defined in (2.15). Both the code and the carrier phase measurements are corrupted by the same error sources, but there are three important differences:

- the noise term ε_ϕ is generally lower than the code noise ε_p, making phase observations more accurate (typical values of ε_ϕ are 1 to 5 mm);
- the ionospheric delay I_ϕ has a minus sign, due to the different behaviour of phase and code during ionospheric propagation;
- there is an additional unknown, the integer ambiguity N.

In order to take advantage of the increased precision of these measurements, the integer ambiguity has to be solved. In addition, as will be detailed below, N remains constant as long as the carrier tracking loop maintains the lock on the signal. Any break in the tracking could unpredictably change this value.

Doppler measurements

The Doppler measurement is the instantaneous rate of change of the carrier phase. It is a result of the relative motion between user and satellite, and is important for navigation purposes, since it facilitates the determination of the velocity of the moving receiver. In addition, Doppler measurements can be used in carrier phase measurements for cycle slip detection and correction [79].

Carrier smoothing

Noisy and unambiguous code measurements can be combined with precise and ambiguous carrier measurements. In particular, delta pseudo-ranges and their high precision can be exploited to *smooth* code based pseudo-ranges, with a process referred as carrier smoothing [4].

First, the carrier phase, represented in units of cycles, in (6.20), is represented in units of length, like code phase measurements:

$$\Phi(t) = \lambda\phi(t) = r(t, t-\tau) - I_\phi(t) + T_\phi(t) + c\,(\delta t_u(t) - \delta t^s(t-\tau)) + \lambda N + \varepsilon_\Phi(t)\,. \tag{6.21}$$

Then, an intermediate measure, called *ionosphere-free pseudo-range*, is defined:

$$\rho_{IF}(t) = r(t, t-\tau) + c\,(\delta t_u(t) - \delta t^s(t-\tau)) + T(t)\,. \tag{6.22}$$

The code measurement of (2.15) and the carrier phase measurement of (6.21) can be rewritten as

$$\rho(t) = \rho_{IF}(t) + I(t) + \varepsilon_\rho(t) \tag{6.23}$$

$$\Phi(t) = \rho_{IF}(t) - I(t) + \lambda N + \varepsilon_\Phi(t) \tag{6.24}$$

At this point, the change in the measurements between two measurements epochs, namely t_{i-1} and t_i, is computed:

$$\Delta\rho(t_i) = \rho(t_i) - \rho(t_{i-1}) = \Delta\rho_{IF}(t_i) + \Delta I(t_i) + \Delta\varepsilon_\rho(t_1) \tag{6.25}$$

$$\Delta\Phi(t_i) = \Phi(t_i) - \Phi(t_{i-1}) = \Delta\rho_{IF}(t_i) - \Delta I(t_i) + \Delta\varepsilon_\Phi(t_i) \tag{6.26}$$

where the prefix Δ indicates the change between consecutive epochs. A few considerations can be drawn. First, it has to be reminded that the noise term in the first equation is at metre level, while in the second equation at centimetre level. Second, the integer ambiguity term N disappears,

provided that no cycle clips occur between epochs i and $i-1$. In this way the unknown is eliminated from the system of equations. Then, the terms ΔI can be dropped, assuming that they assume a value near zero, if the measurements epochs are close enough. In this way it is possible to use the value of $\Delta\rho_{IF}(t_i)$ as an accurate estimate of $\Delta\rho_{IF}(t_i)$. In this way it is possible to construct the pseudo-range profile using the carrier-derived delta pseudo-ranges.

In order to proceed in an iterative way, an estimate of the pseudo-range at the beginning of the tracking, denoted epoch 0, is required. It can be computed at each epoch i, as suggested in [4], as

$$\hat{\rho}(t_0)_i = \rho(t_i) - [\Phi(t_i) - \Phi(t_0)] \; . \tag{6.27}$$

This value represents an estimate, because of the presence of code and phase noise and of the ionospheric terms. However, the noise impact can be reduced by averaging the estimate over n epochs:

$$\bar{\rho}(t_0) = \frac{1}{n} \sum_i \hat{\rho}(t_0)_i \, . \tag{6.28}$$

The final smoothed pseudorange profile can then be computed as

$$\bar{\rho}(t_i) = \bar{\rho}(t_0) + [\Phi(t_i) - \Phi(t_0)] \; . \tag{6.29}$$

More complex schemes can be introduced, for example filtering and weighting the contributions of carrier phase and code phase measurements. Note that ant change in the ionosphere between measurement epochs has been disregarded. While this change can be neglected when the two epochs are close enough, in the order of a few seconds, it becomes significant over larger time intervals. Moreover, since the ionospheric term has opposite sign in the code and phase domains, this effect will be doubled when combining code and carrier measurements.. This effect is known as code-carrier divergence, and results in a bias in the final measurement error [4].

6.1.2 A software based PLL

A software routine is implemented in SDR to measure the carrier phase. The steps carrier out by a software PLL are reported hereafter [78].

1. A receiver acquires phase lock with the satellite signal.
2. The initial fractional phase difference between the received and the locally-generated signal in number of cycles in measured:

$$\phi_0(t) = \text{rem}\left(\theta_{RX}(0) - \theta_{loc}(0), 2\pi\right) \; . \tag{6.30}$$

3. From then on, at each instant t, the PLL tracks the change in this measurements by:
   (a) counting the number of full carrier cycles:

$$N_c(t) = \lfloor \left(\theta_{RX}(t) - 2\pi\phi_0\right) / \left(2\pi\right) \rfloor \, ; \tag{6.31}$$

   (b) keeping track of the fractional cycle at each epoch in fraction of cycles:

$$\phi_{\text{rem}}(t) = \text{rem}\left(\theta_{RX}(t) - 2\pi\phi_0, \, 2\pi\right) \; . \tag{6.32}$$

   This happens for every $t = kT_c$ with $k = 1,2,\ldots$.
4. Finally the carrier phase measurement in cycles can be written as:

$$\phi(t) = N_c(t) + \phi_{\text{rem}}(t) \tag{6.33}$$

This same scheme is implemented in software according to the code in Listing 6.1:

```
1  % carrier phase measurements
2      if (epoch == 1)
3          AccDoppler = ...
4                  (2*pi*(carrFreq-fIF) .* time) + remFraction(1);
5          remFraction(epoch) = ...
6                  rem( AccDoppler(blksize+1), (2*pi) );
7          remInteger(epoch) = ...
8                  fix( AccDoppler(blksize+1) / (2*pi) );
9      elseif (epoch>1)
10         AccDoppler = ...
11                 (2*pi*(carrFreq-fIF) .* time) + remFraction(epoch-1);
12         remFraction(epoch) = ...
13                 rem( AccDoppler(blksize+1) , (2*pi));
14         remInteger(epoch) = ...
15             remInteger(epoch-1) + fix(AccDoppler(blksize+1) / (2*pi));
16         accumulatedPhase(epoch) = ...
17             accumulatedPhase(epoch-1) + AccDoppler(end);
18     end
```

Listing 6.1: Matlab code for carrier phase measurements

In particular, a few points are underlined.

- The quantity computed in lines 3 and 4 and in lines 10 and 11, called `AccDoppler` is the instantaneous phase of the signal. A phase is computed for each value of the discrete time `t` during the whole integration period. This is computed using the estimate of the Doppler frequency coming from the acquisition or from the previous epoch. Indeed, `carrFreq-fIF` is exactly equal to the Doppler shift estimated by the receiver. Furthermore, in lines 10 and 11, the fractional phase of the previous epoch is added.
- `AccDoppler(blksize+1)` represents the value of the instantaneous phase at the end of the integration period, that is to say for $t = T_c$, since `blksize` is the size in samples of an integration period. `AccDoppler(blksize+1)` in the pseudo-code corresponds exactly to the value $\theta_{RX}(t)$ in (6.31) and (6.32).
- The variable named `remFraction` corresponds to the variable ϕ_{rem} of (6.32).
- The variable named `remInteger` corresponds to the variable N_c of (6.31) accumulated over time.

In particular we underline that:

- the quantity computed in lines 3 and 4 and in lines 10 and 11, called `AccDoppler` is the instantaneous phase of the signal. A phase is computed for each value of the discrete time `t` during the whole integration period. This is computed using the estimate of the Doppler frequency coming from the acquisition or from the previous epoch. Indeed, `carrFreq-fIF` is exactly equal to the Doppler shift estimated by the receiver. Furthermore, in lines 10 and 11, the fractional phase of the previous epoch is added.
- `AccDoppler(blksize+1)` represents the value of the instantaneous phase at the end of the integration period, that is to say for $t = T_{int}$, since `blksize` is the size in samples of an integration period. `AccDoppler(blksize+1)` in the pseudo-code corresponds exactly to the value $\theta_{RX}(t)$ in (6.31) and (6.32).

- the variable named `remFraction` corresponds to the variable ϕ_{rem} of (6.32)
- the variable named `remInteger` corresponds to the variable N_c of (6.31) accumulated over time

In order to better understand these quantities, their values as obtained running the Matlab routine with N-FUELS generated signals is reported in the following. First a signal with Doppler frequency equal to 0 Hz + 1 Hz/s is considered. In this case (Figure 6.2) the Doppler is low, and

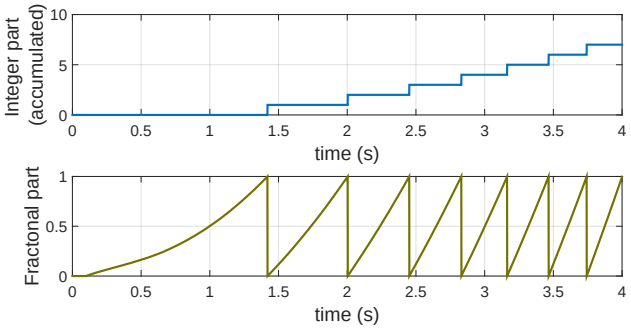

Figure 6.2: Cycles count ($T_c = 1$ ms).

for each epoch the phase increment is very limited, largely below 1 full cycle.

In a second example, a signal characterized by Doppler equal to 5000 Hz + 1 Hz/s is considered. Results are reported in Figure 6.3a, and are similar to the ones in Figure 6.2, with the exception of the scale of the y-axis. In 4 seconds more than 20 000 cycles are counted. This means that in a single integration epoch (1 ms), the satellites moves so fast that more than one full cycle passes. Therefore the integer counter assumes values larger than one.

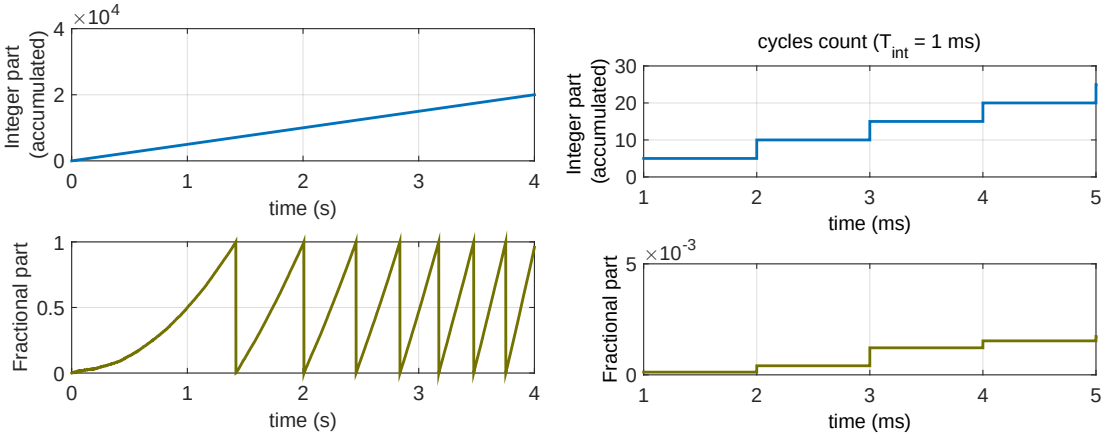

(a) Cycles count. **(b)** Cycles count (enlargement).

Figure 6.3: Cycles count ($T_c = 1$ ms), high dynamic.

Figure 6.3b shows an enlargement of Figure 6.3a, depicting this fact. It is clear how in one integration time (1 ms) about 5 full cycles pass. This proves that the PLL can count an integer number of cycles larger than 1.

Indeed, the PLL does not really measures the instantaneous phase at the end of the integration epoch. The output of the discriminator is some quantity close the instantaneous phase at half the integration period. Then, this value enters the loop filter as input and is combined with previous measurements properly weighted. The output value is indeed a frequency, corresponding to the estimated Doppler frequency (in the code, `codeFreq`). This frequency is then used to update the value of the NCO. By using this value we are able to compute the instantaneous phase at the end of the integration epoch, not modulo 2π. This instantaneous phase at the end of the integration epoch not modulo 2π contains the information of the integer number of cycles and on the fractional number of cycles. The integer number of cycles is computed according to (6.31), the fractional number of cycles, i.e. the instantaneous phase modulo 2π at the end of the integration epoch, according to (6.32).

A real PLL does not update the phase

Despite their name, PLLs are not really tracking the phase of the signal. It is better to say they the track the average instantaneous phase of the signal, which indeed corresponds to the instantaneous phase of the signal at half the integration period. Let's assume that the phase, considering the notation of (6.2), is time variant. Thus, during one complete integration epoch, it assumes different values. The discriminator of the loop, such as the arctangent, has the task to produce an estimate of the phase of the signal:

$$\phi[n] = \operatorname{atan} 2 \left(I[n], Q[n] \right) . \tag{6.34}$$

Nevertheless, being the phase time-variant, the estimate corresponds to an average of the different values of the instantaneous phase. It can be proved that this average corresponds to the instantaneous phase at half the integration epoch.

Successively, this information is used only to derive a frequency. Exploiting the fact the frequency is the derivative of the phase, a value of the frequency is derived by means of a difference quotient between two consecutive measurements. The frequency at epoch n can be computed as:

$$f[n] = \frac{1}{2\pi} \frac{\phi[n] - \phi[n-1]}{T_c} \tag{6.35}$$

This value of the frequency is finally used to update the NCO for the wipe-off in the following epoch. It has not be said that more complex equation than the one in (6.35) can be used, to reduce impact of noise and to account for larger dynamics and stresses.

Therefore, we can state that a PLL tracks the average phase, but uses a the phase rate, i.e. the frequency, to close the loop, by updating the NCO. This approach may seem wrong or not complete. How can a loop completely track a signal characterized by frequency and phase by just using the frequency? The answer is in the fact that frequency and phase are connected, exactly by the relationship of (6.2). A continuous stretching and de-stretching of the signal, obtained by varying the frequency of the NCO at each epoch, assures a good tracking. In other words, the frequency of the local signal is increased or decreased in order to recover the initial phase difference. This fact is depicted in Figure 6.4.

A second approach is to compute both the frequency and the instantaneous phase at the end of the integration epoch, and to build a local signal with the same frequency and starting with an initial instantaneous phase equal to the final phase, both estimated at the previous epoch.

6.1.3 The problem of the Doppler rate when simulating the input signal

The generation of a GNSS signal requires to pay attention to the definition of the frequency. When dealing with a non constant Doppler frequency, that is to say with a frequency rate, a problem may

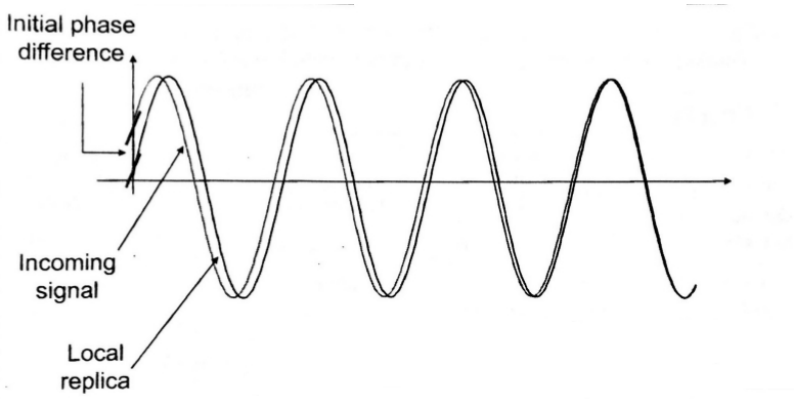

Figure 6.4: Phase recovered by adjusting the phase rate in a PLL [28].

arise, due to two possible definitions of the frequency of a GNSS signal. In general, for a real GNSS receiver, the Doppler frequency is not constant, because of three combined effects: the satellite motion; the clocks instabilities; and the eventual receiver motion. Despite being very small, this Doppler rate has to be taken into account.

Let's first consider a generic GNSS signal of the type

$$x(t) = \cos\left(2\pi f t + \varphi\right) , \tag{6.36}$$

where f is the frequency of the sinusoid and φ is the initial phase. This expression is correct as long as the frequency f is constant, and therefore equal to the inverse of the period T of the sinusoidal signal.

One may want to introduce a time varying frequency, which can be simply expressed as the sum of a constant component and a linear component

$$f(t) = f_{IF} + f_{\text{cost}} + \alpha t \, , \tag{6.37}$$

where f_{IF} is the known down-conversion intermediate frequency, and α corresponds to the slope of the linear component. The frequency rate is defined as the first derivative of the frequency with respect to time, that is

$$\dot{f}(t) = \frac{df(t)}{dt} = \alpha \, . \tag{6.38}$$

Consequently, the frequency rate is equal to α. By simply substituting the expression of the time varying frequency (6.37) in the expression of the signal (6.36), the following expression is obtained:

$$x(t) = \cos\left[2\pi \left(f_{IF} + f_{\text{cost}} + \alpha t\right) t + \varphi\right] , \tag{6.39}$$

Then, it is possible to compute the instantaneous frequency of the signal, according to the definition of the instantaneous frequency as derivative of the instantaneous phase (Section 6.1.1).

$$\begin{aligned} f_{ist}(t) &= \frac{1}{2\pi}\frac{d}{dt}\varphi_{ist}(t) \\ &= \frac{1}{2\pi}\frac{d}{dt}\left[2\pi \left(f_{IF} + f_{\text{cost}} + \alpha t\right) t + \varphi\right] \\ &= \frac{d}{dt}\left[f_{IF} t + f_{\text{cost}} t + \alpha t^2\right] \\ &= f_{IF} + f_{\text{cost}} + 2\alpha t \, . \end{aligned} \tag{6.40}$$

Because of the derivative of the quadratic term αt^2, a term 2 appears. Surprisingly, the instantaneous frequency computed in (6.40) differs from the time varying frequency defined in (6.37).

This is due to the wrong definition of frequency as inverse of the period. The error occurs when (6.37) is substituted in (6.36). The correct substitution, according to the definitions of Section 6.1.1, requires to insert in the expression of the generic signal the instantaneous phase:

$$x(t) = \cos\left[\varphi_{ist}(t)\right] . \tag{6.41}$$

Since the instantaneous frequency corresponds to the derivative of the instantaneous phase, the instantaneous phase can be found by integrating the instantaneous frequency:

$$\varphi_{ist}(t) = 2\pi \int_o^t f(t)\, dt\,. \tag{6.42}$$

In the specific case of (6.37),

$$\begin{aligned}\varphi_{ist}(t) &= 2\pi \int_o^t f_{IF} + f_{\text{cost}} + \alpha t\, dt \\ &= 2\pi \left(f_{IF} t + f_{\text{cost}} t + \alpha \frac{t^2}{2} \right) \\ &= 2\pi \left(f_{IF} + f_{\text{cost}} + \frac{1}{2}\alpha t \right) t\,. \end{aligned} \tag{6.43}$$

Then, by substituting the instantaneous phase of (6.43) in the generic signal, the following expression is obtained:

$$\tilde{x}(t) = \cos\left[2\pi \left(f_{IF} + f_{\text{cost}} + \frac{1}{2}\alpha t \right) t \right] , \tag{6.44}$$

which differs from the signal obtained in (6.39) by a factor of 1/2 in the linear term. The second formulation is more correct. This can be proved by computing the instantaneous frequency, as done before in (6.40).

$$\begin{aligned} f_{ist}(t) &= \frac{1}{2\pi}\frac{d}{dt}\left[2\pi \left(f_{IF} + f_{\text{cost}} + \frac{1}{2}\alpha t \right) t + \varphi \right] \\ &= \frac{d}{dt}\left[f_{IF} t + f_{\text{cost}} t + \frac{1}{2}\alpha t^2 \right] \\ &= f_{IF} + f_{\text{cost}} + \alpha t\,. \end{aligned} \tag{6.45}$$

This value of the instantaneous frequency exactly matches with the value of the time-varying frequency defined in (6.37). Therefore, this second formulation should be used when generating GNSS signals.

6.2 The problem of cycle slips

Cycle slips are problems affecting in principle each type of communication receiver, including a carrier synchronizer. In particular, [80] provides a good description of the cycle slip in general purpose digital communication receivers: what happens is that when the signal constellation is invariant under a rotation of angle p, the carrier synchronizer cannot distinguish between an angle θ and an angle $\theta + kp$, with $k \in \mathbb{N}$. For example, in the case of legacy GPS signals employing a BPSK modulation and an arctan discriminator, we have $p = \pi$. Therefore the carrier synchronizer has infinitely many stable operating points, spaced by π.

During stable working conditions, the carrier phase estimate exhibits small random fluctuations around a stable operating point. This effect is mainly caused by the noise affecting the receiver and to the errors introduced by the channel. In general this is not a problem, since the fluctuations are small with respect to the linear region of the discriminator; in addition, the tracking loop is specifically designed to take into account these oscillations and to correct the estimate, thus converging towards the stable point. However, occasionally noise or other disturbances may push the estimate far away from the current stable operating point, into the domain of attraction of a neighbouring stable operating point. This introduces an ambiguity in the measurements, because the tracking loop is in principle not able to detect this effect. This phenomenon is known as **cycle slip** and is illustrated in Figure 6.5.

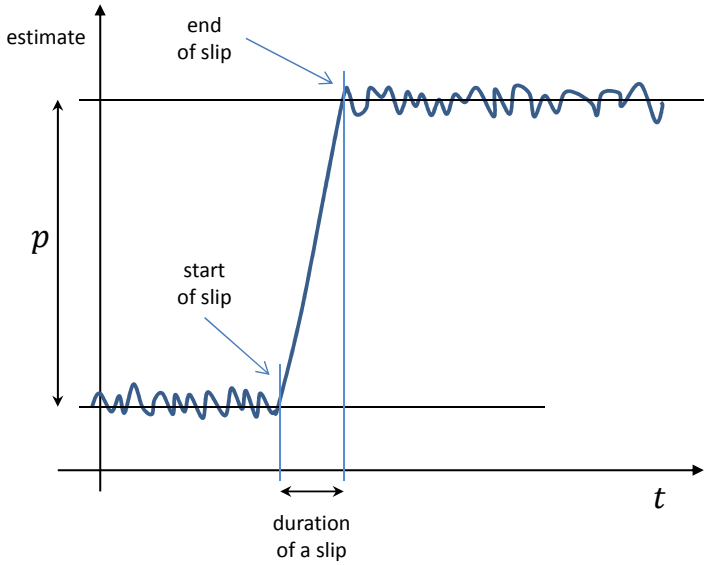

Figure 6.5: Illustration of cycle slips (citemeyr1998digital.

The figure shows the trend of a generic estimate, such as the carrier phase, affected by small fluctuations. At the start of the slip, the estimate is pushed away by a quantity p, but since this new value is stable, the receiver is not able, unless specifically designed to do this, to detect the slip, and continues tracking the signal. Even if the ambiguity is usually referred to in units of full carrier cycles, there may be an additional half-cycle ambiguity due to the navigation message modulated on the signals [81]. It is important to underline also that the occurrence of a cycle slip affects not only the current measurement, but also the following epochs [82].

The most dangerous consequence described in literature, concerning cycle slips, is the introduction of burst of symbol errors. A simple solution, suggested by [80], is based on the monitoring of a known synchronization world or through differential encoding/decoding. Nevertheless, this cannot be realized in real-time (since the error can be recovered only at the end of the synchronization word).

6.2.1 Cycle slips in GNSS

Detection and correction of cycle slips is one of key problems of GNSS receivers dealing with carrier phase measurements [83]. Cycle slips are indeed the biggest GPS error sources if they remain in the raw carrier phase measurements, leading to biased estimates for the navigation parameters [84, 85].

In navigation receivers, the concept of cycle slip is connected to carrier phase measurements in the PLLs, as described in [86]. These are discontinuities in the time series of carrier-phase measurements due to the receiver temporarily losing lock on the carrier of a GNSS signal caused by signal blockage [87]. Any time a receiver is turned on, the PLL tracks the signal and observes the fractional part of the phase, that is to say the difference between the satellite transmitted signal carrier and the local replica. At the same time, an integer counter, representing the number of accumulated carrier phase cycles, is initialized: during the tracking phase, whenever the fractional phase changes from 2π to 0 the counter is incremented by one. The initial integer number of cycles N between the satellite and the receiver is unknown, although constant. However, if a signal lock occurs, a jump in the instantaneous accumulated phase is experienced, as depicted in Figure 6.6, between t_i and t_{i+1}. In this case the real number of accumulated cycles increments by an integer number, while the value of the counter does not change.

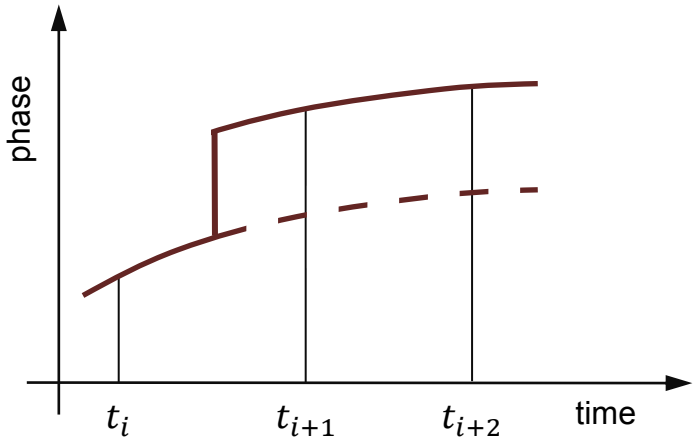

Figure 6.6: Graphical representation of a cycle slip [86].

6.2.2 Causes of cycle slips

According to literature, cycle slips may arise in different scenarios and are caused by different sources.

- **Obstruction** of the line-of-sight path between the receiver and the satellite. This is due to any kind of obstacles, such as trees, buildings, bridges, mountains, ans so on [17, 86, 83, 85]. This is the most common type and this is why we see more slips in kinematic environment data than static one [79].
- **Low** C/N_0 of the SIS at the receiver, due to bad ionospheric conditions, high dynamics of the receiver, multipath, or low satellite elevation [17, 86, 83, 85].
- Excessive large unpredictable **Doppler** effect due to receiver motion [22].
- **Errors** or bugs in the receiver software, which can lead to incorrect signal processing [86, 85].
- **Multipath**, in specific case in which the reflected signal is stronger than the direct signal [17].
- Malfunctioning of the satellite **oscillators**, although very rare [86, 83].

In any event, a loss of carrier phase measurement continuity, no matter how brief, results in an unknown loss of carrier cycles when the signal is re-tracked by the receiver and in a new unknown ambiguity to be solved [17]. As claimed in [17], allowing corrupted carrier-phase measurements to propagate forward usually causes immediate loss of the fixed solution.

6.2.3 Detection and mitigation strategies

According to literature review, the processing of cycle-slips is conventionally composed by four sequential stages [88]:

1. cycle-slip **detection**, which checks the occurrence of a cycle-slip;
2. cycle-slip **determination**, which quantifies the size of the cycle-slip;
3. cycle-slip **validation**, which tests the correctness of the calculated cycle-slip size;
4. cycle-slip **removal**, which removes the cycle-slip from the phase measurement.

The cycle-slip detection has to be invoked epoch-by-epoch to check the discontinuity of carrier phase data [89]. For the sake of computational efficiency, the cycle-slip detection should be a rapid algorithm. As an alternative, it is also possible to avoid determination, validation and removal, and to pass directly from the detection state to the mitigation step. In fact, mitigation does not require the knowledge of the slip size. This approach is easier but in general less accurate.

Once a cycle slip is detected, it can be handled in two ways. One way is to repair the slip. The other way is to reinitialize the unknown ambiguity parameter in the phase measurements. The former technique requires an exact estimation of the size of the slip but could be done instantaneously. The latter solution is more secure, but it is time-consuming and computationally intensive [87].

Several detection methods are proposed in literature, based on different techniques (polynomial extrapolation, multi-times differential, ionosphere residual, filtering, wavelet) and with different characteristics in terms of detection probability, complexity, computational burden, etc. In addition, a distinction between single frequency and dual/triple frequency methods can be made. Options of cycle slip detection are also dependent on the dynamics (static or kinematic); it is more difficult to detect a slip while in kinematic positioning than in static, because of the additional Doppler shift created by the motion, as reported in Figure 6.7. The ambiguity resolution is even more challenging in real-time navigation due to receiver dynamics and the time-sensitive nature of the required kinematic solution. Therefore, it would save effort and time to detect and estimate the size of cycle slips and correct the measurements accordingly instead of resorting to a new ambiguity resolution [87].

6.3 Artificial generation of slips

An experimental analysis has been carried out in order to asses the problems of cycle slips in a GNSS receiver. In particular a Matlab GNSS receiver [32] has been used and modified.

The main problem to face when dealing with cycle slips is to force a cycle slip. Indeed, a cycle slip is not a property of the received signal, but rather is related to the way it is processed, as will be outlined later on. A cycle slip can be induced in a receiver by processing signals with certain nuisances. Exploiting N-FUELS (Section A.1), first regular signals, characterized by standard Doppler and C/N_0 profiles, are generated and collected. Then, the same signals are generated, by adding some nuisances, in terms of sudden, unexpected and limited outages at a given instant. These outages can consist for example of a power drop or of a not expected Doppler frequency

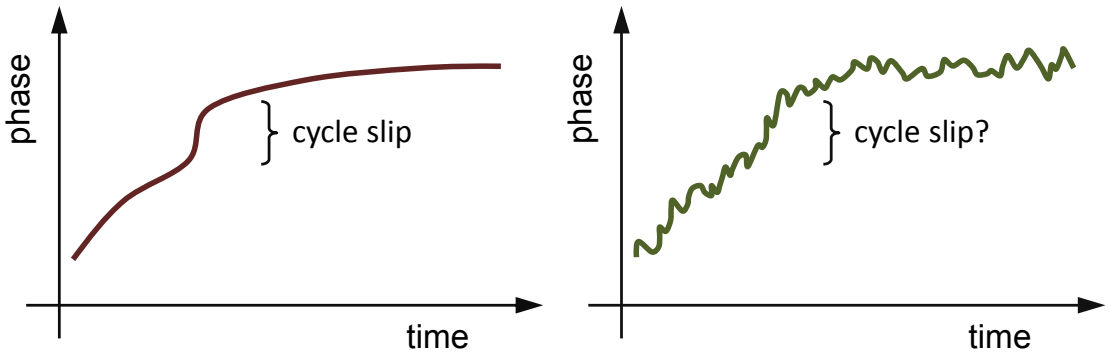

(a) Static **(b)** Kinematic

Figure 6.7: Static vs. kinematic cycle slip phase behaviour and detection.

trend. In this way, a temporary tracking error, causing cycle clips, can be experienced. Then, a simple tracking loop can be configured to count the cycles, and by comparing the results of the processing of these signals, it is possible to assess the presence of cycle slips. The number of carrier cycles is computed inside the tracking loop according to the algorithm reported in the pseudo-code of Listing 6.1. The error in terms of accumulated phase can also be computed.

6.3.1 Signal affected by a constant Doppler

A first simulation has been carried out with a signal characterized by a constant C/N_0 equal to 50 dBHz and affected by a constant Doppler ($f_D = 200$ Hz). A sudden outage is simulated, after 1.6 s and lasting about 100 ms, as shown in the Doppler and C/N_0 patterns in Figure 6.8.

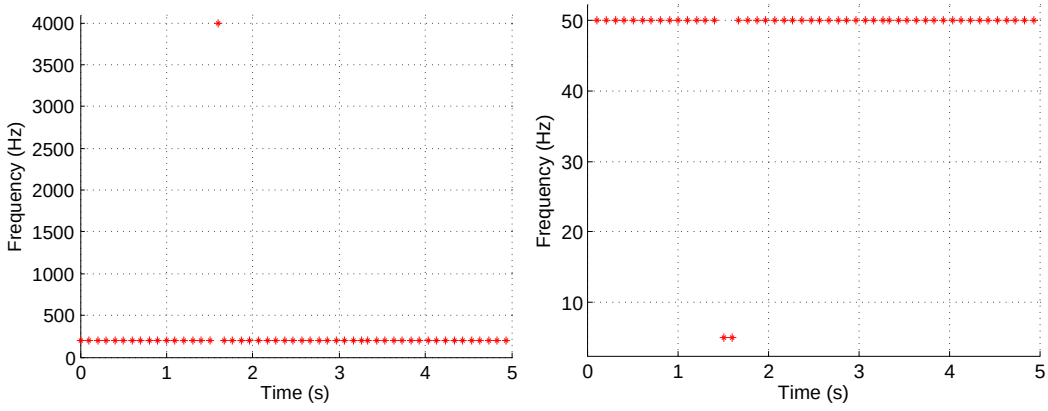

(a) Doppler pattern. **(b)** C/N_0 pattern.

Figure 6.8: Patterns used for the generation of a cycle slip affected data set.

It is has been proved that a receiver tracking stage loses temporary the lock when processing this signal. Results are shown in Figure 6.9. The DLL fails during this interval, the P, L and E correlators go to 0 for a small amount of time following the signal outage and the C/N_0 estimator

fails. However, despite the bad signal conditions, the tracking loop it is still able to recover after the outage, avoiding a LOL and a new re-acquisition, but introducing the possibility of a cycle slip.

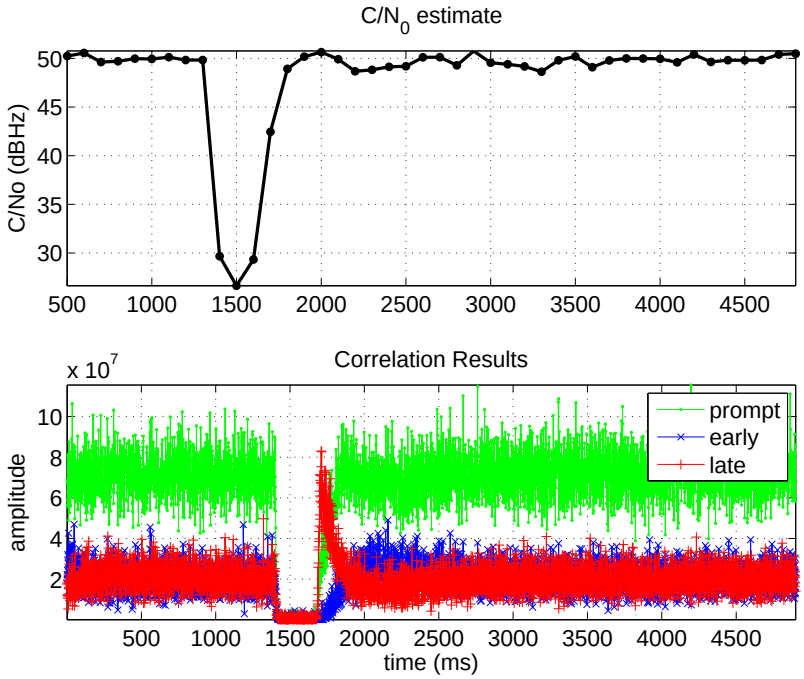

Figure 6.9: DLL correlations results and C/N_0 estimate in presence of forced signal errors.

In order to understand whether a cycle slip has occurred or not, a comparison is drawn, considering the results obtained processing another N-FUELS signal, not affected by any outage. Figure 6.10 shows the result of the simulation, in terms of carrier phase cycles count. The lines represent the number of integer cycles accumulated since the PLL start; in particular the red line corresponds to the outage-free signal, while the blue line corresponds to the signal affected by a nuisances.

The results are consistent with the expectations. In fact, as reported above, at around 1.6 s a cycle clip has been artificially created. The carrier cycles in the nuisance-free signal increase with a rate equal to 200 cycles/s, that corresponds to the estimated increase due to the Doppler frequency equal to 200 Hz:

$$\phi(t) = \int_0^t f_D(\tau)\, d\tau = \int_{0\text{ s}}^{1\text{ s}} 200\text{ Hz}\, d\tau = 200\text{ cycles}\,. \tag{6.46}$$

The enlargements show that before $t = 1.6$ s the count related to the two signals is identical. As expected, from 1.6 s on, there are errors in the count of the cycles in the outage-affected signal (blue line), that are much more evident as long as time passes. In particular, in this case, the difference is exactly of one cycle, as confirmed by Figure 6.11, depicting the difference between the two counters in number of cycles.

Moreover, the correspondence between code and phase observations can be proved. From the Doppler frequency f_D it is possible to compute the relative velocity between receiver and satellite:

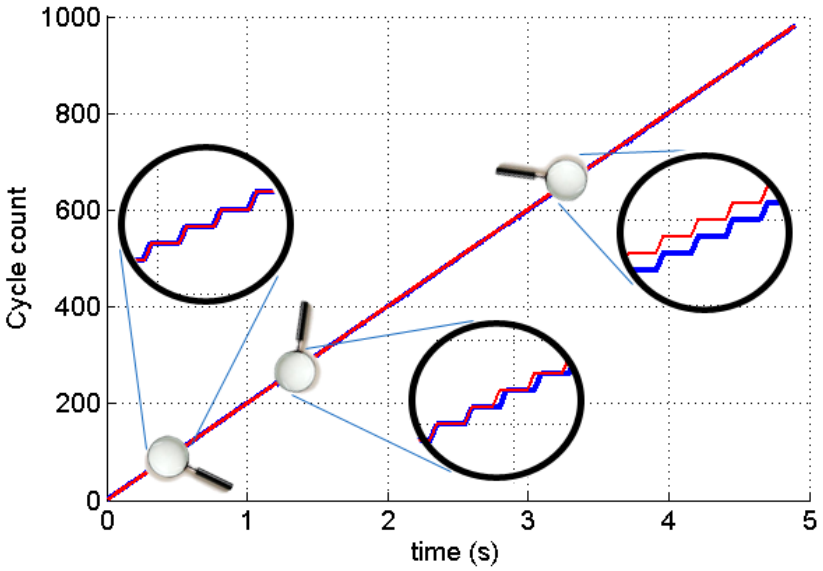

Figure 6.10: Carrier phase cycle count in absence and presence of cycle slips.

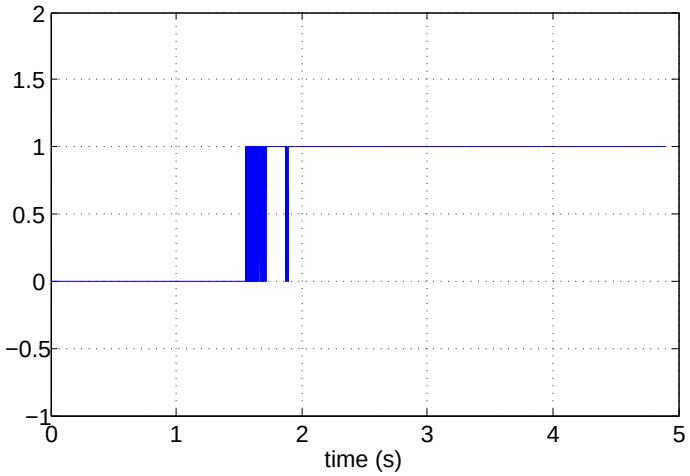

Figure 6.11: Carrier phase cycle count difference with respect to Figure 6.10.

$$\begin{aligned} v_0 &= c\left(1 - \frac{f_{L1}}{f_{L1} + f_D}\right) \\ &\simeq 3 \times 10^8 \left(1 - \frac{1575.42\ \text{MHz}}{1575.42\ \text{MHz} + 200\ \text{Hz}}\right) \simeq 38\ \text{m/s}\,. \end{aligned} \tag{6.47}$$

Therefore, during a period of 5 s the relative distance between receiver and satellite, computed from Doppler measurements, is equal to

$$r_D = v_o t = 38\ \text{m/s} \cdot 5\ \text{s} = 190\ \text{m}\,. \tag{6.48}$$

A similar rough result can be found from the carrier phase cycle count measurement:

$$r_P = \phi\lambda_{L1} \simeq 1000 \text{ cycles} \cdot 0.19 \text{ m} = 190 \text{ m}\,. \tag{6.49}$$

6.3.2 Signal affected by an increasing Doppler frequency

A more severe cycle slip phenomenon can be experienced with any combination of the following factors.

- A linear increasing Doppler profile; in fact, if the Doppler frequency follows a linear trend with respect to time, the carrier phase cycle count exhibits a quadratic trend, and the effect of a single cycle slip is more dangerous.
- A higher Doppler frequency; in fact, if the Doppler frequency is higher, the wavelength is lower, and therefore the probability of experiencing a slip is larger.
- A longer outage period, causing a longer outage at the receivers.

A new set of signals has been generated with N-FUELS, characterized by the parameters reported in Table 6.1.

Table 6.1: Summary of the N-FUELS signals characteristics used in the simulation.

	C/N_0	f_D
No cycle slip	50 dBHz	1500 Hz + 50 Hz/s
Weak cycle slip	50 dBHz and 5 dBHz from 1.5 to 1.7 s	1500 Hz + 50 Hz/s and −5000 Hz from 1.5 to 1.6 s
Strong cycle slip	50 dBHz and 5 dBHz from 1.5 to 1.7 s	1500 Hz + 50 Hz/s and −5000 Hz from 1.5 to 1.7 s

Figure 6.12 shows the carrier phase cycle count for the three signals described in Table 6.1. It is clear, looking at the three enlargements, that while in the first part (up to 1.6 s) the count for the three cases is identical. At about $t = 1.6$ s the effect of the power and frequency changes in the input signals begins to be evident, and a small difference in the cycle count, with respect to the corresponding nuisance-free signals, is present. At the end of the processing, the errors in the cycle count are much bigger.

Figure 6.13a and 6.13b show the difference in the cycle count with respect to time between the reference nuisance-free signal and the two corrupted signals respectively. In the first case the difference oscillates between 1 and 2 cycles, while in the second case it reaches 10 cycles. Moreover, it has been experimented that using a larger noise equivalent bandwidth the error in the cycle count increases, as more noise enters the receiver. This fact confirms that cycle slip are generated by the receiver signal processing. In particular, for the GPS L1 signal, an error in the cycle count of 10 cycles leads to an error in the pseudo-range of $10 \cdot 19$ cm $\simeq 2$ m, which for precise centimetre level positioning is very dangerous.

6.3.3 Impact of the C/N_0 and of the Doppler frequency changes

In order to assess whether the main impact in the error in the cycle count is due to the sudden drop of the signal power or to the sudden change of the Doppler frequency, a new set of signal have been generated:

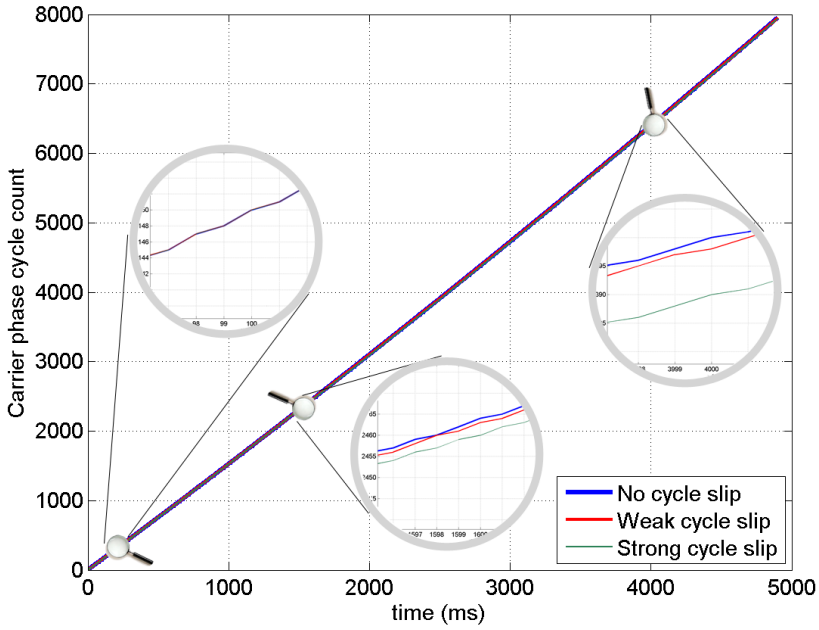

Figure 6.12: Carrier phase cycle count in the absence and in the presence of weak and strong cycle slips.

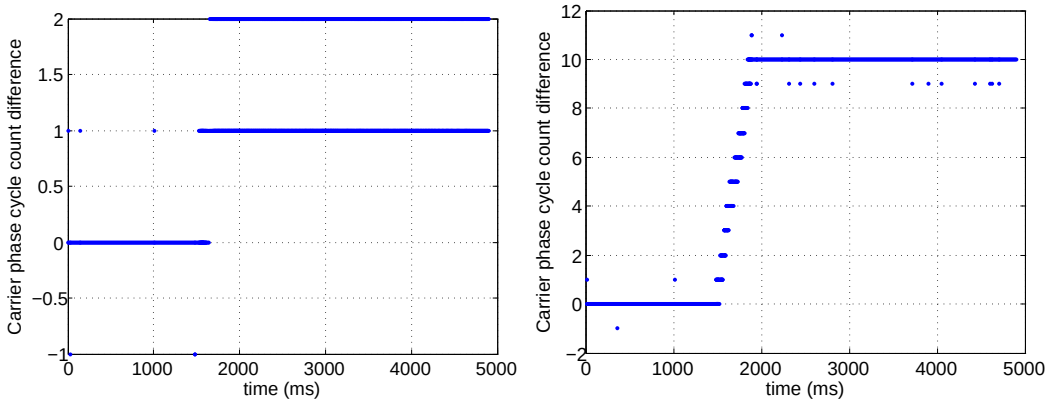

(a) Weak cycle slip **(b)** Strong cycle slip

Figure 6.13: Carrier phase cycle count difference in presence of cycle slips with respect to a clean signal.

- a nuisance-free signal, identical to the one described in Section 6.3.2, with constant C/N_0 and linear increasing Doppler frequency;
- a signal affected by a constant C/N_0, identical to the one of the nuisance-free signal, and a sudden Doppler frequency change;

- a signal affected by a linear increasing Doppler frequency, identical to the one of the outage-free signal, and a sudden power drop.

The three files have been tested in the same way, counting the carrier phase cycles. As expected, cycle slips occurs in the second and in the third signal, but their impact is different. Figure 6.14 shows the count for the three different signals. A power drop introduces a small error in the cycle count, approximately of 1 cycle, while the Doppler frequency change introduces errors of several cycles.

Therefore it is assumed that the main cause of the cycle slips described above is the change in the Doppler frequency in the input signal.

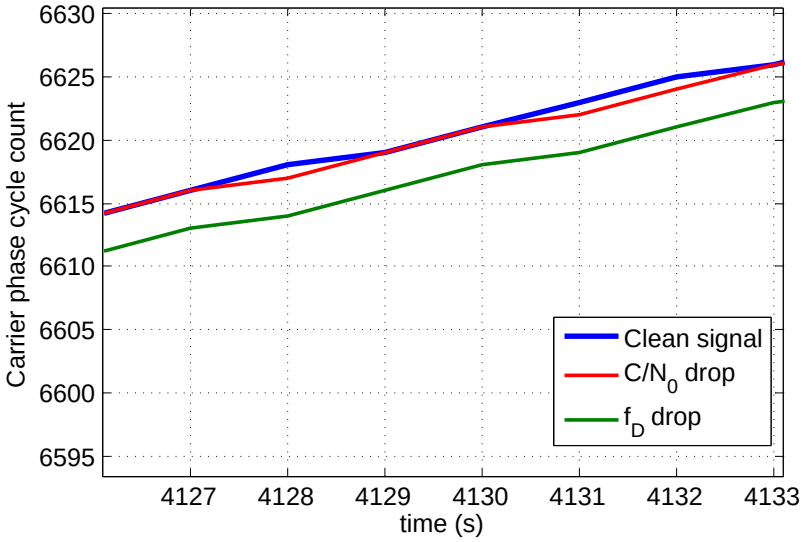

Figure 6.14: Carrier phase cycle count in the absence and in the presence of strong cycle slips, distinctly due to C/N_0 drop and Doppler change.

6.3.4 Impact of a longer Doppler drop interval

By increasing the length of the outage period, different results are obtained. As already outlined, the size of the count error increases with the outage length. However, when this time interval value exceeds a certain threshold, the PLL is no longer able to maintain the lock, and a LOL is experienced. Of course in this case a new acquisition is needed, and therefore a new ambiguity resolution process has to be initialized.

Figure 6.15 shows the cycle count of a clean signal and of a signal with the same outages described in Section 6.3.2 but lasting 1 s instead of 100 ms. Since an outage occurs, the cycle count is completely wrong, and it has to be reinitialized.

6.3.5 PLL only results

In a standard GNSS receiver a concatenated PLL/DLL structure is normally employed. It is theoretically expected that the effect of Doppler frequency variations impacts more on the PLL than on the DLL. In other words, the DLL, which correctly works, ignoring the signal variations, can help the PLL. In order to test the behaviour of a PLL only implementation, a GNSS signal containing no modulation (no navigation data and no PRN code) has been generated with N-FUELS. A

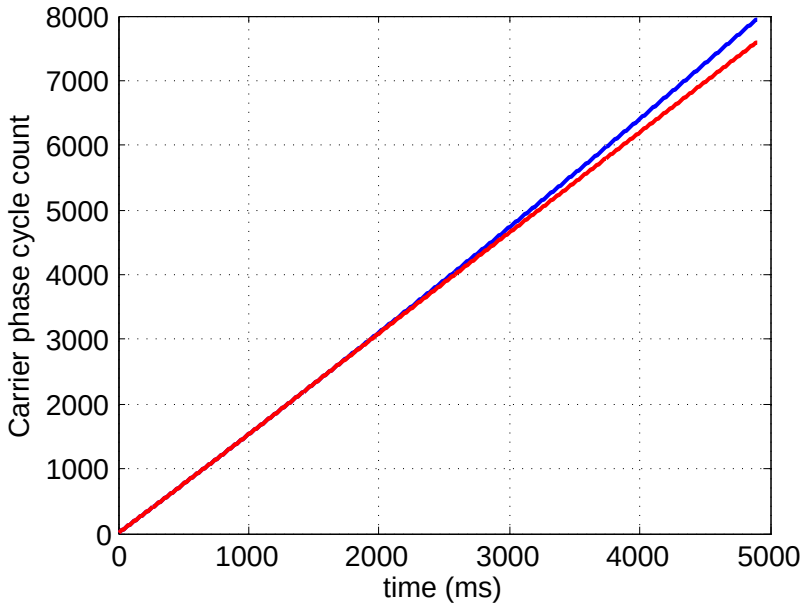

Figure 6.15: Carrier phase cycle count in absence and presence of long cycle slips.

modified version of the receiver has been used, containing only a PLL, with an equivalent noise bandwidth of 50 Hz. As in the last example, only a Doppler frequency drop has been introduced.

The prompt I and Q correlators relative to this signal are shown in Figure 6.16. As expected, all the power is contained in the I correlator, which assumes always positive values, since no modulations are present. After 1.6 s the alterations of the input signal introduce some errors in the PLL; however, no LOL is experienced and after 0.2 s the PLL restarts working normally.

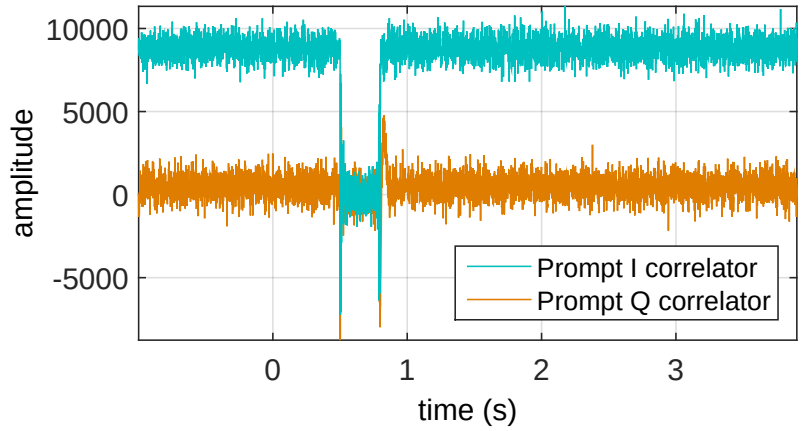

Figure 6.16: Prompt I and Q correlators for a PLL tracking only a carrier with no modulation.

The error in the number of cycle counted is similar to the results of the full DLL/PLL concatenated structure. Figure 6.17a shows the carrier phase cycle count for two signals considered. It is clear, looking at the three enlargements, that while in the first part (up to $t = 1.6$ s) the count for the two cases is identical, around $t = 1.6$ s the effect of the frequency change begins to be evident,

and a small difference in the cycle count is present. Finally, around $t = 4$ s the errors in the cycle count are much bigger, leading to significant errors.

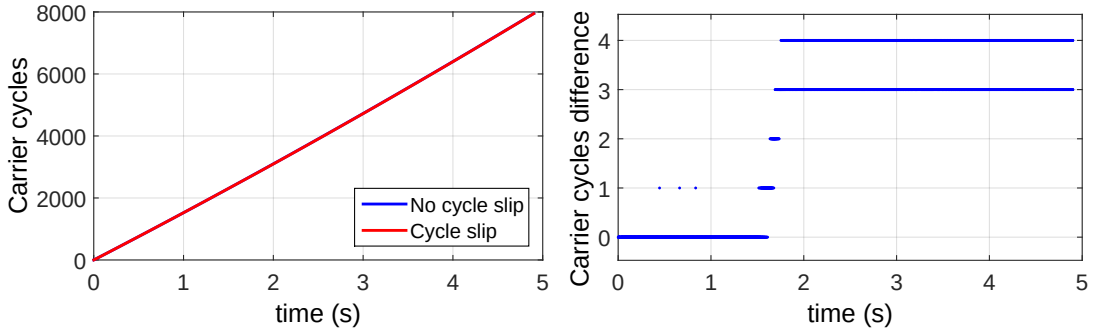

(a) Cycles count **(b)** Cycles difference

Figure 6.17: Carrier phase cycle count in absence and presence of cycle slips for PLL only loops.

Figure 6.17b shows the difference in the cycle count with respect to time between the two signals. The difference oscillates between 3 and 4 cycles.

6.3.6 Impact of C/N_0 drops

In this section, the effect of C/N_0 drops is evaluated. The nominal C/N_0 is set equal to 50 dBHz for all the 5 s of simulation in the nuisance-free signal. A drop to 0 dBHz is introduced in the outage-signal, in order to account for a temporary signal shadowing and to trigger a cycle slip in the receiver. In particular the C/N_0 profile is reported in Figure 6.18. The common signal parameters are reported in Table 6.2.

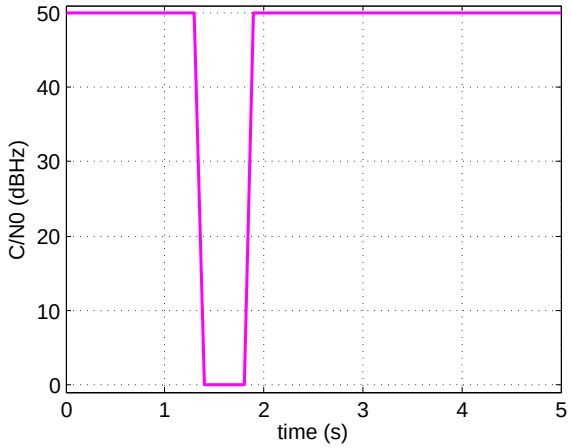

Figure 6.18: C/N_0 profile as generated by the N-FUELS signal generator.

Results of the standard processing are reported in Figure 6.19. The DLL and PLL noise bandwidth are respectively equal to 2 Hz and 10 Hz. The Doppler frequency is equal to 0 Hz + 1 Hz/s The DLL correlators spacing is set to 0.5 chip. As expected, in the regular case the tracking is good and exhibits no problems. On the other hand, the tracking of the second signal yields to

Table 6.2: Summary of N-FUELS parameters.

Signal length	5 s
IF carrier frequency	4.1304 MHz
Sampling frequency	16.3676 MHz
IF carrier phase	0.215 rad
Number of satellites	1
Modulation	GPS L1
PRN code	1
Code delay	0.02 ms
Doppler profile	linear
Doppler rate	1 Hz/s or 10 Hz/s
Initial Doppler frequency	0 Hz or 1000 Hz
Navigation message	present
Quantization	4 bits
C/N_0	50 dBHz
Front-end filter	Butterworth, 4th order, $B = 4.092$ MHz
Format	int8

some interesting facts. The tracking is initially good, until about 1.3 s. Then clearly, the signal power goes below the receiver sensitivity, and the signal is no longer tracked. However, after the 0.5 seconds of nuisance, the receiver goes back to the tracking stage, without the need to re-acquire the signal. This is because the signal dynamics are limited, and the signal parameters, such as code delay and Doppler frequency, even after an outage of half a second still lie within the loops pull-in regions. For this reason this cannot be considered a LOL, since in some way the lock is maintained and no re-acquisition is needed.

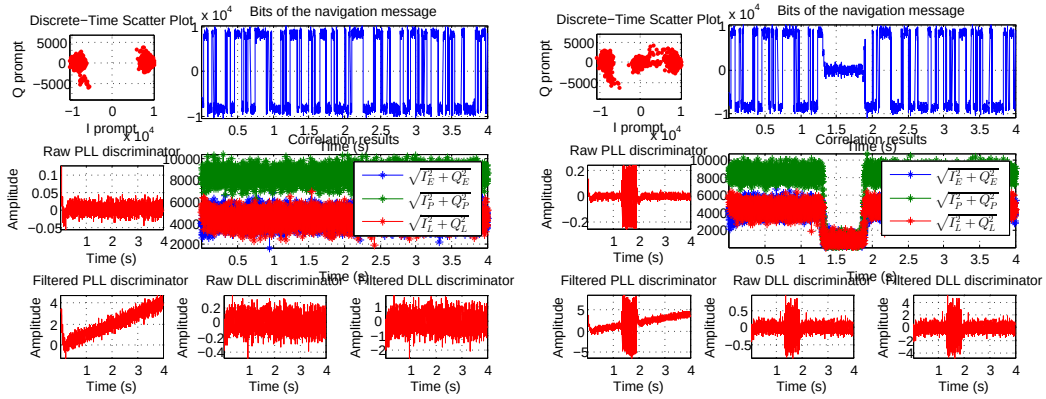

(a) Regular signal **(b)** Nuisance affected signal

Figure 6.19: Output of signal tracking.

This fact in principle is not so dangerous for a GNSS receiver working on code measurements. By contrast, it is deleterious when considering phase measurements, because during the outage period it is not possible to observe and accumulate the phase, and jumps of cycles are likely to occur.

By looking at the integer and fractional phase as measured by the receivers, the presence of cycle slips can be evaluated. In particular, the sum of the integer count plus the fractional count

in unit of cycles is evaluated in both cases, and then compared by means of a difference. It is assumed that in the first case the cycle count is correct, and thus the difference with the second case represents the number of cycles "slipped". Figure 6.20a shows the cycle count in the two cases. While the blue line, corresponding to the cycle-slip free processing, exhibits a smooth trend, the red curve shows some irregularity in correspondence of the C/N_0 drop. Nevertheless, when the tracking goes back to the steady state, the cycle count restarts correctly. This is because during the signal shadowing, less that a full cycle passes. Similarly, Figure 6.20b shows the difference in cycles between the two curves plotted in Figure 6.20a. As expected, after some spikes during the signal outage period, it is equal to zero.

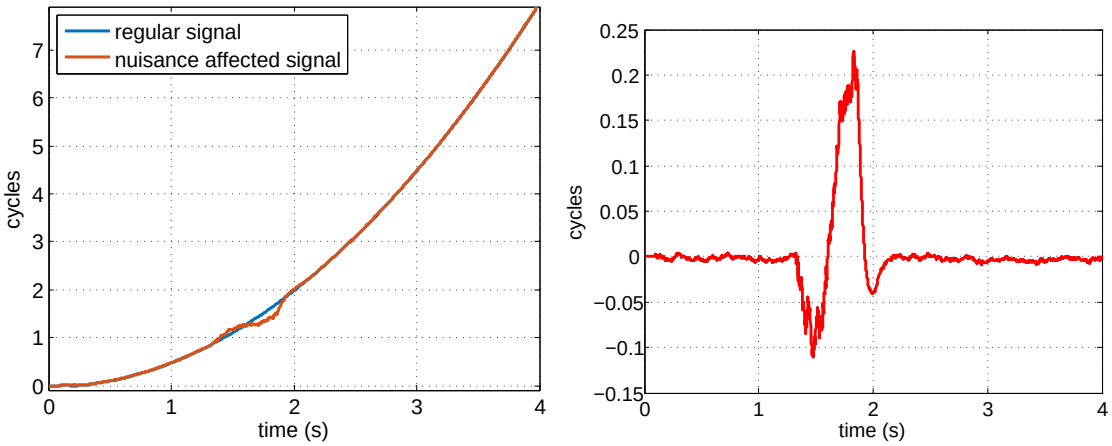

(a) Cycles count **(b)** Cycles difference

Figure 6.20: Cycle count along 3 seconds of processing for two different input signals.

It has been proved that a cycle slip may occur at least in the following three cases:

1. a lower PLL bandwidth;
2. a larger instantaneous Doppler frequency in absolute value;
3. a higher Doppler rate.

These three cases share a common point: the fact that during the outage period the signal parameters change too much with respect to the capabilities of the loop. Thus a cycle slip is induced, as clarified in the following sections.

Effect of the PLL bandwidth

When changing the PLL bandwidth, two main effects arise.

- By reducing the bandwidth, the pull-in region decreases, and lower dynamics can be accounted for. At the same time, in order to track signal with high dynamics, a larger bandwidth should be used.
- By increasing the bandwidth, more noise enters the loop, thus reducing its sensitivity; a lower bandwidth assures better noise rejection capabilities.

It is evident that a trade-off should be considered.

In this particular case, with respect to the result in Figure 6.20, the PLL bandwidth is reduced from 10 Hz to 2 Hz. Results are reported in Figure 6.21. Clearly the blue curve in Figure 6.21a has the same trend of the blue curve in Figure 6.20a. What differs is the red curve; the consequence of reducing the bandwidth is that the pull-in region is lower as well, and therefore, as soon as the outage period finishes and the loop properly tracks the signal again, it locks on a different stability point, spaced by π with respect to the previous one, thus creating a difference in the cycle count of half a cycle. This is better depicted in Figure 6.21b. This result further confirms that the presence of a cycle slip strictly depends on the receiver architecture.

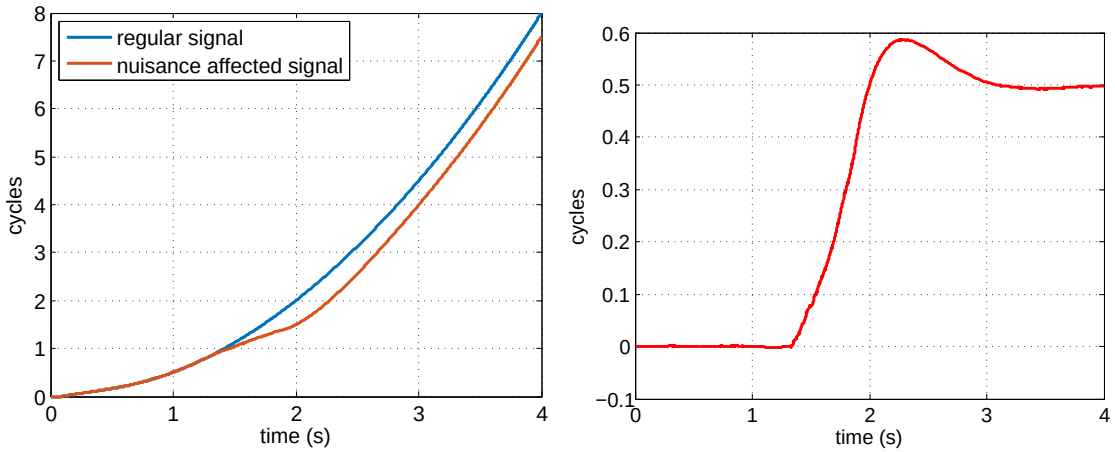

(a) Cycles count **(b)** Cycles difference

Figure 6.21: Effect of the bandwidth, cycles count for $B_{\mathbf{PLL}} = 2$ Hz.

It can be proved that by using a value of 20 Hz for the PLL bandwidth, no cycle slips are obtained. On the other hand, a bandwidth of 1 Hz does not allow a proper tracking.

Effect of the instantaneous Doppler frequency

A similar effect happens when the instantaneous frequency is larger in absolute value. The results are reported in Figure 6.22 for a PLL bandwidth of 10 Hz. This arises from the fact that the phase is the integral of the frequency. Therefore, supposing the the outage period lasts from $\tau_1 = 1.4$ s to $\tau_2 = 1.8$ s, in the case reported above the total number of cycles in the outage interval is:

$$\int_{\tau_1}^{\tau_2} f_D(\tau)\, d\tau = \int_{1.4}^{1.8} 0 + 1\tau\, d\tau = \left.\frac{t^2}{2}\right|_{1.4}^{1.8} = 0.64 \text{ cycles}\,. \tag{6.50}$$

On the contrary, in the case of a signal with $f_D = 1000$ Hz $+ 1$ Hz/s as in this simulation, the total number of cycles in the same outage interval is:

$$\int_{\tau_1}^{\tau_2} f_D(\tau)\, d\tau = \int_{1.4}^{1.8} 1000 + 1\tau\, d\tau = 1000\tau + \left.\frac{t^2}{2}\right|_{1.4}^{1.8} = 400.64 \text{ cycles}\,. \tag{6.51}$$

This huge number justifies the possibility to lose half a cycle during the outage period. In particular, Figure 6.22a reports the cycle count for the reference and the nuisance-affected signals, with a magnifying on two regions, respectively before and after the C/N_0 drop. Similarly, Figure 6.22b reports the difference between the two curves, outlining a cycle slip of half a cycle.

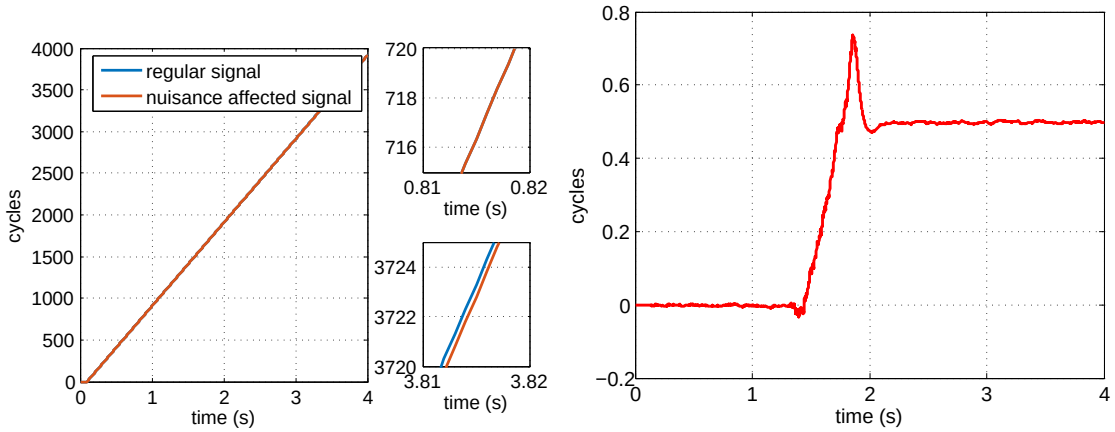

(a) Cycles count **(b)** Cycles difference

Figure 6.22: Effect of the Doppler frequency, cycles count for $f_0 = 1000$ Hz.

It can be proved that by reducing the bandwidth to 2 Hz, a cycle slip of half a cycle is obtained, whereas by increasing it to 20 Hz a cycle slip of 1 cycle is obtained.

Effect of the Doppler rate

Finally, cycle slips are obtained when the Doppler rate is pushed to high values, that is to say in high dynamics environments.

First a simulation with $f_D = 0$ Hz $+ 10$ Hz/s is run, then a similar case with $f_D = 1000$ Hz $+ 10$ Hz/s, both with a bandwidth of 10 Hz. The results are reported in Figure 6.23 and Figure 6.24. The amount of the slip corresponds to one and one and a half cycles respectively.

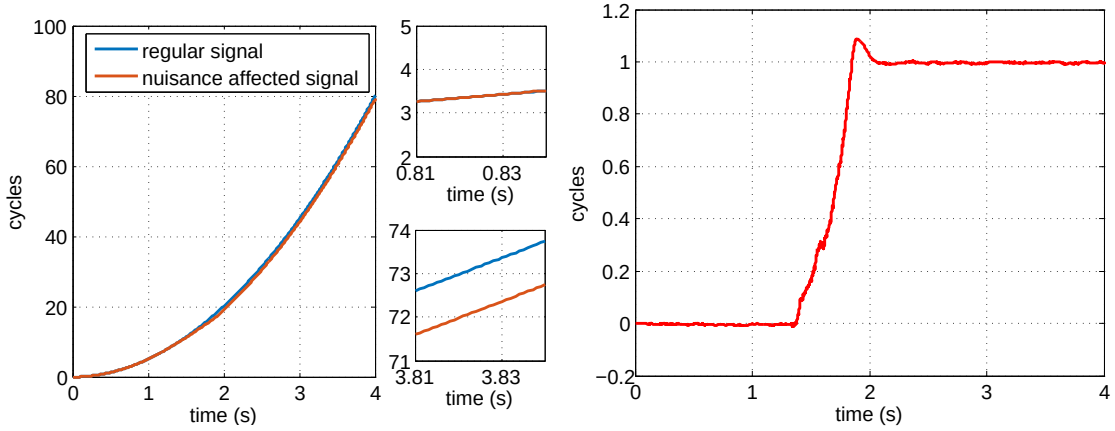

(a) Cycles count **(b)** Cycles difference

Figure 6.23: Effect of the Doppler frequency, cycles count for $f_0 = 0$ Hz $+ 10$ Hz/s.

Summarizing, it has been proved that the cycle slip phenomenon does not appear under every condition. The error in the cycle count is more evident if:

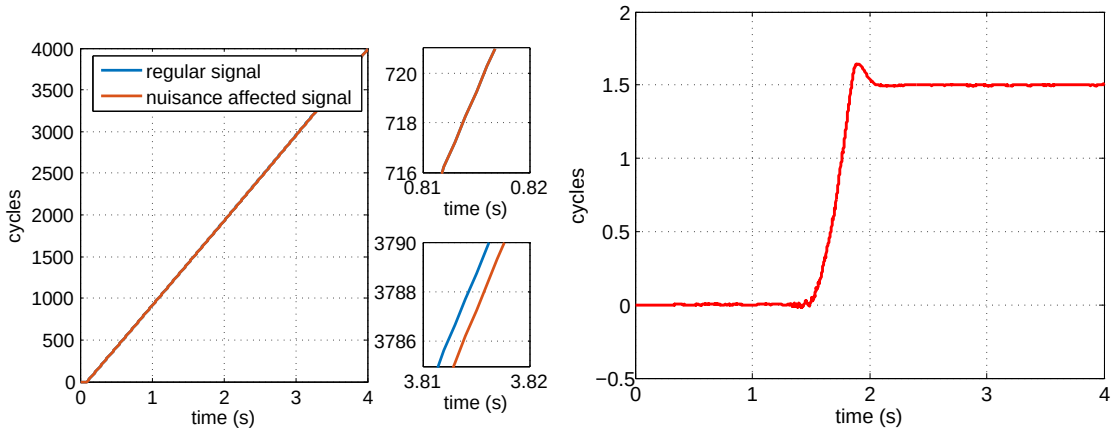

(a) Cycles count **(b)** Cycles difference

Figure 6.24: Effect of the Doppler frequency, cycles count for $f_0 = 1000$ Hz $+ 10$ Hz/s.

- the Doppler frequency affecting the GNSS signal is high (in absolute value);
- the Doppler frequency rate is higher;
- the errors introduced in the input signal are stronger;
- the errors introduced affect the signal for a longer time interval;
- the PLL bandwidth is lower;

Chapter 7

Doppler and Doppler Rate Analysis

In this section the maximum value for the Doppler and the Doppler rate in a typical dynamic environment are derived, both for GPS L1 C/A and Galileo E1 signals. Theoretically, also the clock instability introduces a frequency shift that can be considered as additional Doppler; however this aspect is neglected in this analysis. A complete analysis of the phenomenon in the static case can be found in [19].

7.1 Signal and system model

The simplified geometry concerning the system model is reported in Figure 7.1. The radius of the Earth is about 6378 km around the equator and about 6357 km passing through the poles. Thus the average radius, r_e, can be considered equal to 6368 km. The radius of the satellite orbit, r_s depends on the constellations. It is equal to 26 560 km for GPS and to 29 600 km for Galileo. Consequently, the distance from the Earth surface, r_h, can be computed. This corresponds to the shortest distance between a user on the surface of the Earth and the satellite, which occurs at the zenith (elevation angle of 90 degrees).

In GPS and Galileo, the orbits are nearly circular, and the orbital period can then be calculated as

$$T_{\text{circ}} = 2\pi\sqrt{\frac{a^3}{GM}}\,, \tag{7.1}$$

where a is the semi-major axis (equals the radius) of the orbit, and GM is the product of the gravitational constant and the mass of the Earth. In World Geodetic System 1984 (WGS84), the value of GM is $3.986004418 \times 10^{14}$ m^3/s^2. The orbital period corresponds to about 43 080 seconds or 11 hours and 58 minutes for GPS and to about 50 680 seconds or 14 hours and 5 minutes for Galileo. Knowing the mean orbital radius, the *angular velocity* $d\theta/\,dt$ of a generic satellite can be calculated as

$$\frac{d\theta}{dt} \simeq \frac{2\pi}{T_{\text{circ}}} \tag{7.2}$$

and the *tangential velocity* v_s as

$$v_s = r_s \frac{d\theta}{dt}\,, \tag{7.3}$$

that gives $v_s = 3\,874$ m/s for GPS and $v_s = 3\,670$ m/s for Galileo.

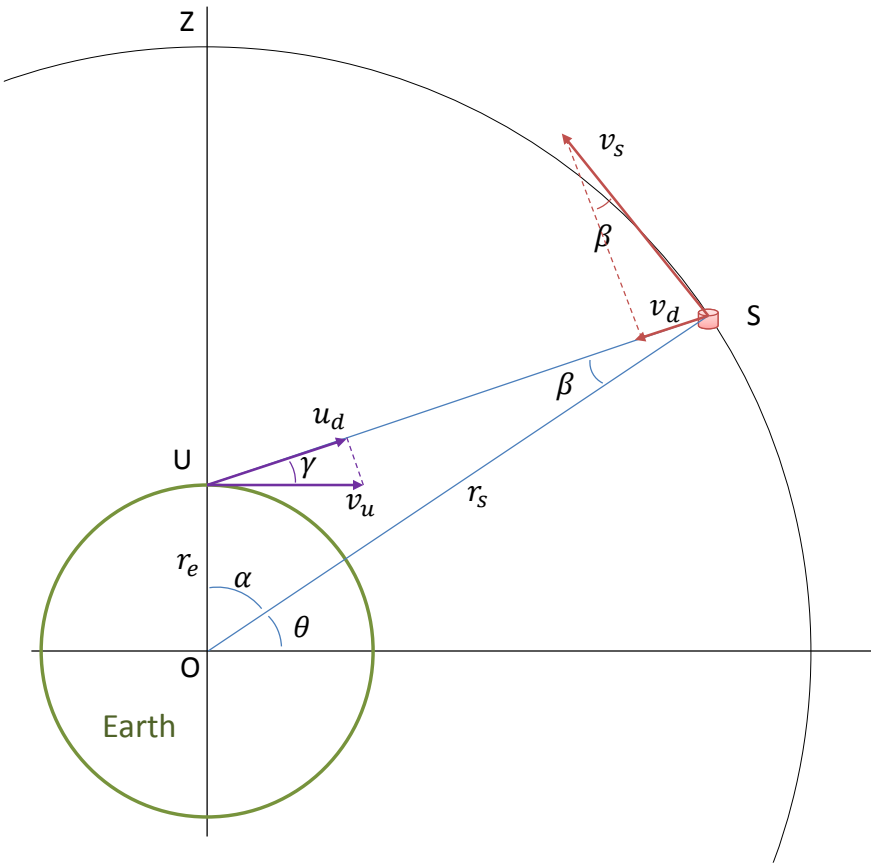

Figure 7.1: Representation of Earth, user and satellite geometry.

The Doppler shift is caused by the satellite velocity component denoted *radial velocity*, v_d toward the user:

$$v_d = v_s \sin\beta\,. \tag{7.4}$$

By exploiting trigonometric identities, and referring to Figure 7.1, $\sin\beta$ can be expressed as

$$\sin\beta = \frac{r_e \cos\theta}{\overline{US}}\,. \tag{7.5}$$

Similarly, the segment $\overline{US}$ can be computed as

$$\overline{US} = \sqrt{r_e^2 + r_s^2 - 2r_e r_s \sin\theta}\,, \tag{7.6}$$

and therefore, merging (7.4), (7.5) and (7.6) and

$$v_d = \frac{v_s r_e \cos\theta}{\sqrt{r_e^2 + r_s^2 - 2r_e r_s \sin\theta}}\,. \tag{7.7}$$

In the dynamics scenario also the user dynamic has to be accounted for. In order to simplify the problem, the following two assumptions can be made:

- the user U is travelling on a flat surface, on the sea level;
- the user U is travelling at a constant speed, its acceleration is null.

The speed of the user is denoted v_u, and according to the first assumption, it corresponds to its tangential velocity. As for the satellite, only the component in the direction of the satellite contributes to the Doppler shift. Therefore, the velocity component in the direction of the satellite is computed. In addition, the worst case is considered, that is to say, the case of a user moving towards the satellite in the situation in which the satellite is moving towards the user.

Given a tangential velocity v_d, the component toward the satellite u_d can be computed as (referring to Figure 7.1):

$$u_d = v_u \cos\gamma \,. \tag{7.8}$$

Exploiting the law of sines, it can be stated that:

$$\frac{r_s}{\sin\left(\frac{\pi}{2}+\gamma\right)} = \frac{\overline{US}}{\sin\alpha} \,. \tag{7.9}$$

Since $\sin\left(\frac{\pi}{2}+\gamma\right) = \cos\gamma$, (7.9) can be rewritten solving for $\cos\gamma$:

$$\cos\gamma = \frac{r_s}{\overline{US}}\sin\alpha = \frac{r_s}{\overline{US}}\cos\left(\frac{\pi}{2}-\alpha\right) = \frac{r_s}{\overline{US}}\cos\theta \,. \tag{7.10}$$

Finally, combining (7.8), (7.10) and (7.6), the expression of the user Doppler component is found:

$$u_d = v_u \frac{r_s\cos\theta}{\sqrt{r_e^2 + r_s^2 - 2r_e r_s \sin\theta}} \,. \tag{7.11}$$

The total velocity contributing to the Doppler shifts then the sum of the component due to satellite motion v_d and of the component due to user motion u_d:

$$\begin{aligned} v &= v_d + u_d \\ &= \frac{v_s r_e \cos\theta}{\sqrt{r_e^2 + r_s^2 - 2r_e r_s \sin\theta}} + \frac{v_u r_s \cos\theta}{\sqrt{r_e^2 + r_s^2 - 2r_e r_s \sin\theta}} \\ &= \frac{\cos\theta}{\sqrt{r_e^2 + r_s^2 - 2r_e r_s \sin\theta}} \left(v_s r_e + v_u r_s\right) \,. \end{aligned} \tag{7.12}$$

The maximum value of the velocity can be found by deriving (7.12) with respect to the angle θ and setting the result equal to 0.

$$\begin{aligned} \frac{dv}{d\theta} &= \frac{d}{d\theta}\frac{\cos\theta}{\sqrt{r_e^2 + r_s^2 - 2r_e r_s \sin\theta}}\left(v_s r_e + v_u r_s\right) \\ &= \left(v_s r_e + v_u r_s\right)\frac{d}{d\theta}\frac{\cos\theta}{\sqrt{r_e^2 + r_s^2 - 2r_e r_s \sin\theta}} \,. \end{aligned} \tag{7.13}$$

In turn,

$$\begin{aligned}
&\frac{d}{d\theta}\frac{\cos\theta}{\sqrt{r_e^2+r_s^2-2r_e r_s\sin\theta}} = \\
=&\frac{-\sin\theta\sqrt{r_e^2+r_s^2-2r_e r_s\sin\theta}-\cos\theta\frac{-2r_e r_s\cos\theta}{2\sqrt{r_e^2+r_s^2-2r_e r_s\sin\theta}}}{r_e^2+r_s^2-2r_e r_s\sin\theta} = \\
=&\frac{-\sin\theta\sqrt{r_e^2+r_s^2-2r_e r_s\sin\theta}+\frac{r_e r_s\cos^2\theta}{\sqrt{r_e^2+r_s^2-2r_e r_s\sin\theta}}}{r_e^2+r_s^2-2r_e r_s\sin\theta} = \\
=&\frac{-\sin\theta\left(r_e^2+r_s^2-2r_e r_s\sin\theta\right)+r_e r_s\cos^2\theta}{\left(r_e^2+r_s^2-2r_e r_s\sin\theta\right)^{3/2}} = \\
=&\frac{-r_e^2\sin\theta-r_s^2\sin\theta+2r_e r_s\sin^2\theta+r_e r_s\cos^2\theta}{\left(r_e^2+r_s^2-2r_e r_s\sin\theta\right)^{3/2}} = \\
=&\frac{r_e r_s\sin^2\theta-(r_e^2+r_s^2)\sin\theta+r_e r_s}{\left(r_e^2+r_s^2-2r_e r_s\sin\theta\right)^{3/2}}\,.
\end{aligned} \tag{7.14}$$

So, substituting in (7.13),

$$\frac{dv}{d\theta} = (v_s r_e + v_u r_s)\,\frac{r_e r_s\sin^2\theta-(r_e^2+r_s^2)\sin\theta+r_e r_s}{\left(r_e^2+r_s^2-2r_e r_s\sin\theta\right)^{3/2}}\,. \tag{7.15}$$

(7.15) is equal to 0 when its numerator is equal to 0, that is

$$\begin{aligned}
&r_e r_s\sin^2\theta-(r_e^2+r_s^2)\sin\theta+r_e r_s = 0 \\
&\sin\theta = \frac{r_e}{r_s} \quad \text{or} \quad \sin\theta = \frac{r_s}{r_e}\,.
\end{aligned} \tag{7.16}$$

The only real solution is for $\sin\theta = \frac{r_e}{r_s}$ which gives:

$$\theta = \arcsin\left(\frac{r_s}{r_e}\right)\,. \tag{7.17}$$

This value corresponds to the point in which the satellite is at the horizon (lowest elevation angle). In fact, by substituting (7.16) in (7.10) we have:

$$\begin{aligned}
\cos\gamma &= \frac{r_s}{\sqrt{r_e^2+r_s^2-2r_e r_s\sin\theta}}\cos\theta \\
&= \frac{r_s}{\sqrt{r_e^2+r_s^2-2r_e r_s\sin\theta}}\sqrt{1-\sin^2\theta} \\
&= \frac{r_s}{\sqrt{r_e^2+r_s^2-2r_e r_s\frac{r_e}{r_s}}}\sqrt{1-\frac{r_e^2}{r_s^2}} \\
&= \frac{r_s^2\left(r_s^2-r_e^2\right)}{r_s^2\left(r_s^2-r_e^2\right)} \\
&= 1\,,
\end{aligned} \tag{7.18}$$

which gives $\gamma = 0$, that means null elevation on the horizon. In this same case, both the satellite component and the user component are at the maximum. On the other hand, when $\theta = 0$ the Doppler velocity is zero.

7.2 Maximum Doppler shift

At this point it is possible to compute the maximum Doppler shift. First, the maximum velocity due to user and satellite motion, by recalling (7.12), is:

$$\begin{aligned} v_{\max} =& v\big|_{\sin\theta=\frac{r_e}{r_s}} = \\ =& \frac{\cos\theta}{\sqrt{r_e^2+r_s^2-2r_e r_s\sin\theta}}\left(v_s r_e + v_u r_s\right)\Bigg|_{\sin\theta=\frac{r_e}{r_s}} \\ =& \frac{\sqrt{1-\sin^2\theta}}{\sqrt{r_e^2+r_s^2-2r_e r_s\sin\theta}}\left(v_s r_e + v_u r_s\right)\Bigg|_{\sin\theta=\frac{r_e}{r_s}} \\ =& \frac{\sqrt{1-\frac{r_e^2}{r_s^2}}}{\sqrt{r_e^2+r_s^2-2r_e r_s\frac{r_e}{r_s}}}\left(v_s r_e + v_u r_s\right) \\ =& \frac{1}{r_s}\left(v_s r_e + v_u r_s\right) \\ =& \frac{v_s r_e}{r_s} + v_u \,. \end{aligned} \tag{7.19}$$

And, as a consequence, the Doppler shift is equal to:

$$f_D = \frac{f_{RF} v_{\max}}{c} = \frac{f_{RF}}{c}\left(\frac{v_s r_e}{r_s} + v_u\right), \tag{7.20}$$

where f_{RF} is the carrier frequency and c is the speed of light. Considering the particular case of a static user ($v_u = 0$), the following known results are obtained: $f_D = 4.880$ kHz for GPS; and $f_D = 4.148$ kHz for Galileo.

Assuming a moving user, the user speed has to be included in the computations. It is reminded that the worst case is assumed, that is the case in which the user is travelling in the horizontal plane toward the satellite. In other words, the direction of the user is the same of the azimuth of the satellite. Considering for example a car moving at 130 km/h exactly in the direction of the satellite, then the maximum Doppler shift is

$$f_D = \frac{1575.42\times10^6}{2.99\times10^8}\left(\frac{3874\ \cdot\ 6368\times10^3}{26560\times10^3} + 36.11\right) = 5.07 \text{ kHz} \tag{7.21}$$

for GPS and

$$f_D = \frac{1575.42\times10^6}{2.99\times10^8}\left(\frac{3670\ \cdot\ 6368\times10^3}{29600\times10^3} + 36.11\right) = 4.81 \text{ kHz} \tag{7.22}$$

for Galileo.

Summing up, a motion of 130 km/h, which can be considered the maximum speed for a standard user, extends the Doppler frequency of about 4%. Nevertheless, for HS receivers featuring long integration times this aspect be considered and properly handled.

7.3 Maximum Doppler shift rate

Similarly, it is possible to compute the maximum Doppler shift rate. The rate of change of the speed v is not constant and can be found by taking the derivative of v with respect to time as

$$\frac{dv}{dt} = \frac{dv}{d\theta}\frac{d\theta}{dt}\,. \tag{7.23}$$

$\frac{dv}{d\theta}$ has been computed in (7.15), thus recalling (7.2):

$$\frac{dv}{dt} = \frac{2\pi\left(v_s r_e + v_u r_s\right)}{T_{\text{circ}}} \frac{r_e r_s \sin^2\theta - \left(r_e^2 + r_s^2\right)\sin\theta + r_e r_s}{\left(r_e^2 + r_s^2 - 2 r_e r_s \sin\theta\right)^{3/2}} \,. \tag{7.24}$$

The maximum Doppler rate can be found by deriving (7.24) with respect to θ and maximizing it. It can be proved that this happens when $\sin\theta = 1$, that corresponds to $\theta = \frac{\pi}{2}$. In this case

$$\begin{aligned}
\left.\frac{dv}{dt}\right|_{\max} &= \left.\frac{dv}{dt}\right|_{\sin\theta=1} \\
&= \frac{2\pi\left(v_s r_e + v_u r_s\right)}{T_{\text{circ}}} \frac{r_e r_s - r_e^2 - r_s^2 + r_e r_s}{\left(r_e^2 + r_s^2 - 2 r_e r_s\right)^{3/2}} \\
&= \frac{2\pi\left(v_s r_e + v_u r_s\right)}{T_{\text{circ}}} \frac{-\left(r_e^2 + r_s^2 - 2 r_e r_s\right)}{\left(r_e^2 + r_s^2 - 2 r_e r_s\right)^{3/2}} \\
&= \frac{2\pi\left(v_s r_e + v_u r_s\right)}{T_{\text{circ}}} \frac{-1}{\sqrt{\left(r_e^2 + r_s^2 - 2 r_e r_s\right)}} \,,
\end{aligned} \tag{7.25}$$

which gives the value of the maximum Doppler rate as:

$$\dot{f}_D = \frac{f_{RF}}{c} \frac{2\pi\left(v_s r_e + v_u r_s\right)}{T_{\text{circ}}} \frac{-1}{\sqrt{\left(r_e^2 + r_s^2 - 2 r_e r_s\right)}} \,. \tag{7.26}$$

And corresponds, for a static user, to $\dot{f}_D = 0.97$ Hz/s for GPS and to $\dot{f}_D = 0.67$ Hz/s for Galileo.

7.4 Results

Some results concerning the maximum Doppler shift and the maximum Doppler shift rate are reported hereafter.

7.4.1 Maximum Doppler shift

The maximum Doppler shift is obtained when the satellite elevation is equal to zero. For a static user this is equal to 4.880 kHz for GPS and 4.148 kHz for Galileo.

When the user speed increases towards the satellite direction this value increases. The trend is reported, both for GPS and Galileo, in Figure 7.2.

When a different elevation is considered, both the satellite component and the user component are weakened. Figure 7.3 reports the trend of the Doppler shift versus the user velocity and the elevation angle.

7.4.2 Maximum Doppler shift rate

The maximum Doppler shift rate is obtained when the satellite elevation is equal to 90°. For a static user this is equal to 0.97 Hz/s for GPS and 0.67 Hz/s for Galileo. When the user speed increases towards the satellite direction this value increases. The trend is reported, both for GPS and Galileo, in Figure 7.4.

When a different elevation is considered, both the satellite component and the user component are weakened. Figure 7.5 reports the trend of the Doppler shift rate versus the user velocity and the elevation angle.

From these plots a very interesting result can be drawn: Doppler rate values higher than 1 Hz/s are clearly beyond the requirements of standard receivers, even in a dynamic environment.

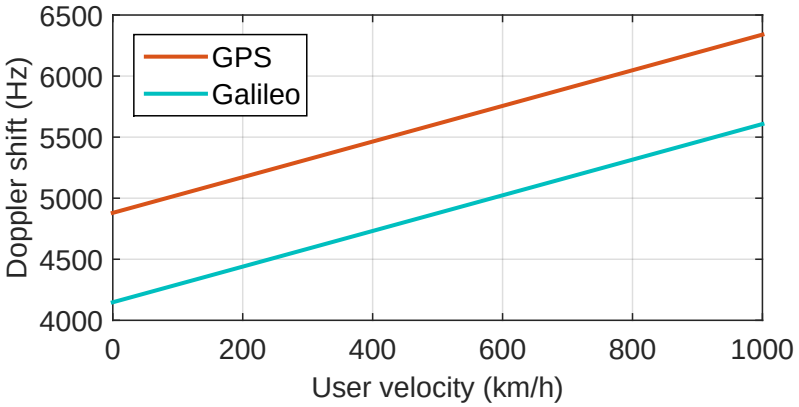

Figure 7.2: Maximum Doppler shift at zero elevation and for different user velocity.

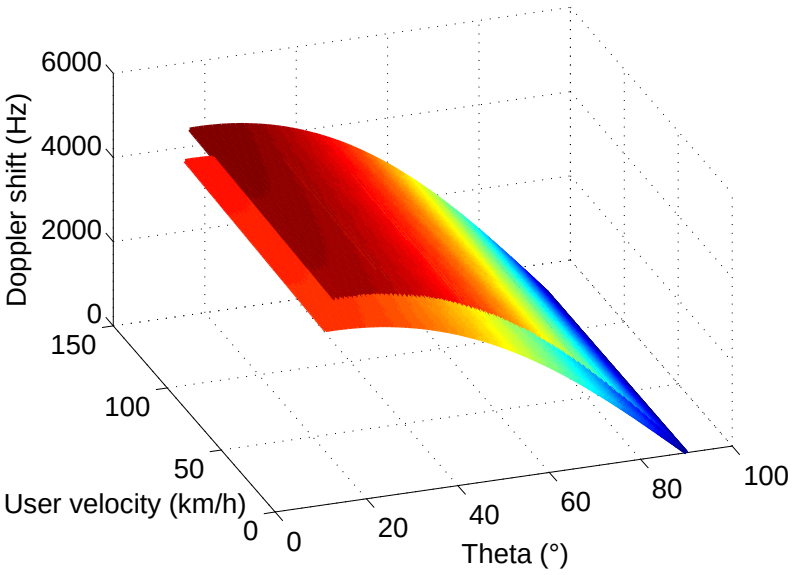

Figure 7.3: Maximum Doppler shift for different elevation angle and user velocity for GPS and Galileo.

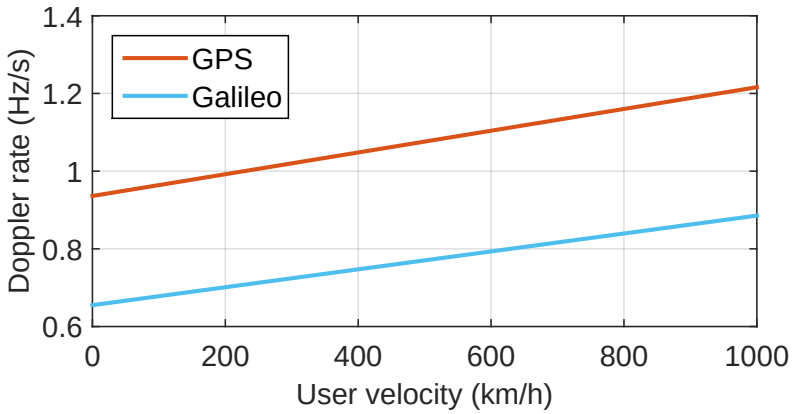

Figure 7.4: Maximum Doppler shift rate at 90° elevation and for different user velocity.

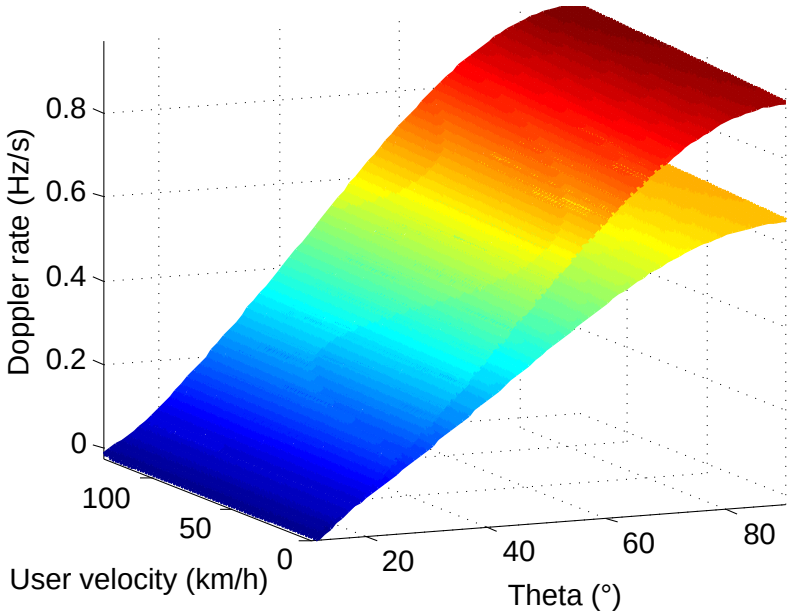

Figure 7.5: Maximum Doppler shift rate for different elevation angle and user velocity for GPS and Galileo.

Chapter 8

Ethical Aspects of GNSS

8.1 Stakeholders network

In Section 1.1 three segments of GNSSs are defined; stakeholders network approximately reflects this partition. The space segment and the control segment are owned by national and international institutions: GPS belongs to the US DoD, while Galileo is being built by the UE and the ESA. In particular, they own the infrastructure, but the use, as for civilian signals (GPS L1 C/A, Galileo E1BC, Galileo E5), is free of charge for the final user. Then the stakeholders network is extended to all the users taking advantage of GNSS signals. From one side, professional devices, used for example in geodesy, represent a niche market, are very expensive and are exploited by a reduced number of people. More interesting for the purpose of this document are commercial and mass-market receivers, produced in very high volume and extremely widespread.

A further distinction can be made between people who use GNSS technology actively and people using it passively. The first case involves for example a tourist using its personal navigation device to reach its hotel, or a person posting a picture in a social network exploiting the geo-referencing features. In all these scenarios the user is aware of the use of GNSS, and holds the right to switch it off if desired. On the contrary, in the second case the users are not the primary beneficiary of the positioning technology, and in principle cannot avoid its use. An example is represented by truck drivers, in the case in which their vehicle is equipped with a GNSS receiver, used by the owner of the transportation company to track the position of the goods. Other applications of this technologies are represented by rental car companies, which have used GPS devices since the mid-1990s, by installing systems to give directions. However, at the same time, these tracking services help companies to monitor their vehicles. Also most of the public buses are equipped with GNSS devices, in order to provide to users detailed information on the best paths and waiting times. In the city of Torino this is managed by the 5T (Tecnologie Telematiche Trasporti Traffico Torino) company [90]. The list of possible applications of *passive* GNSS technology can be extended to a wide variety of applications, including also law enforcement and tracking of people, such as Alzheimer's patients, children, parolee and sex offenders, terrorist, as well as employee monitoring [91, 92].

All the applications included in this latter case, denoted *passive* GNSS, potentially poses ethical problems, as discussed in the next section.

8.2 Ethical issues

Using GPS simply as a position, navigation and time assistance device, such in the *active* case described above, poses no ethical problems [93]. This fact reflects two of the most common myths related to GNSS, which need to be instantly debunked. First, it is worth to remember that, strictly considering GNSS signals, mass-market and commercial GNSS devices are one-way communication systems. They only receive signals from the satellites, and there is no way they can communicate something to GNSS satellites. This would require complex, big, power hungry and expensive transmitting antennas. This feature is present only in particular devices, such as for the Galileo Search And Rescue (SAR) service, which incidentally is not yet implemented [94]. Second, it has to be outlined – although trivial to people working in GNSS field, it is still a false belief for part of the GNSS community – that a GNSS satellite does not transmit the position of the user, neither it tracks people. Rather, it broadcasts its own position in space, mainly in terms of orbital parameters and time stamp. Then, the user receiver, exploiting the information coming from at least 4 satellites, is able to compute by itself its position on Earth.

Therefore, ethical issues arise only when location data are transmitted to another device, exploiting other communication channels, different from GPS, or stored for post-processing. [91, 93, 95] report a list of possible scenarios in which ethical questions concerned to this use of Location Based Service (LBS) for tracking people remain unanswered.

- Does a private enterprise require the consent of an subscriber to track a vehicle equipped with a GNSS receiver?
- Does a government or the police force have the right to location information when they suspect illegal activity?
- Do refugees or illegal immigrants have the right to refuse a tracking device imposed by government?
- Is the 24/7/365 monitoring of a parolee's location information ethical?
- What rights does a mentally ill person have to their location data?
- What of employer work-related location monitoring of employees?

Summarizing, it is possible to say that the main ethical issue facing GNSS tracking is related to **privacy**.

In the following, particular focus is given to the specific case of tracking vehicles for control reasons. The term *geoslavery* has been coined and described as the "practice in which one entity, the master, coercively or surreptitiously monitors and exerts control over the physical location of another individual, the slave" [96].

Control means different thinks, as for example speed: employees driving too fast can waste company's fuel, can wear out the vehicle prematurely or drive up insurance rates [97]. A GPS vehicle tracking system can also raise an alert when someone exceeds a pre-set speed limit, or when the vehicle is used after hours and on weekends, or beyond the borders of a region or country. In addition, using info from the GNSS tracking system, each employee's productivity can be quantified and compared. Precise arrival or delivery estimates can be provided for business reasons, because the estimate is based on the actual location of the goods. At the same time, also the employee can benefit. The presence of on-board tracking devices avoids hand-written logs.

In [98] the authors identify several ethical considerations either encouraging (security, productivity, reputation and impact on third parties) or limiting (privacy, accuracy, inconsistency, right to examine records and informed consent) employee location monitoring. An interesting point is

accuracy: GNSSs inherit accuracy limitations and may of course simply malfunction [17]. They can also be subject to incorrect configuration by operators; on April 2, 2014, all GLONASS satellites broadcast corrupt information for 11 hours; this rendered the system completely unusable to all worldwide GLONASS receivers [99]. Inaccuracies of even a few meters can make the difference between an employee being accused of wrongdoing or exonerated.

Furthermore, the problem of jamming should be considered when dealing with GNSS aspects. Jamming refers to the intentional transmission of RF energy in the GNSS band, to hinder the navigation service by masking signals with noise. The malicious objective of jammers is to cause the receiver to lose tracking and impede signal re-acquisition [100]. Although signal radiation on GNSS bandwidth is not legal and jamming attacks can be detected, jamming represents a severe threat for many GNSS-based applications. A driver could for instance switch on a jammer during non legal operations, such as exceeding speed limits, or using the vehicle for personal reasons. Portable devices able to jam the GPS L1 signal are available on line and can be purchased at a very low cost.

Finally, a case study is considered: in June 2013, local and national newspaper reported the news that the drivers of the public transportation company in the provinces of Torino, Alessandria, Cuneo and Asti, Gruppo Trasporti Torinese (GTT), felt controlled by SIS, a system based on GPS for tracking buses [101, 102]. SIS can not only monitor the position of the bus and give live information on the arrival times at each stop, but also checks if and why the bus is late. From a central station, employees can contact the drivers to ask for the reason of the delay, or even give suggestions to make up for it. However, the Italian *Statuto dei lavoratori* (workers' statute) claims that the worker should not be controlled remotely and that any system should be installed with the agreement of the trade unions.

8.3 Alternative scenarios

The definitive question to be asked is: "is the cost of privacy and security worth it?" [103]. In other words, GNSS represents an excellent LBS that can easily provide location and tracking of people and goods. In principle, most of the ethical issues are not related to the technology itself, but more on the way data are handled, thus making GNSS transparent. Any other LBS undergoes almost the same problems.

For this reason, an alternative solutions should be searched not in the frame of location technologies, but directly in the concept of "tracking". Several alternative technologies could offer – with different levels of accuracy, availability, continuity – almost the same services of GNSS; nevertheless, the problem would be unsolved, since is the way the data are handled that arises ethical issues.

In other words, a caregiver could potentially look after a person even without a satellite-based tracker. For example, a GPS device on a bus could be substituted by a fixed infrastructure, a camera or a scanner at each bus stop and traffic light, thus checking the position of the bus at some fixed spots, and not continuously. However, the ethical problems concerning tracking and controlling of people would remain identical.

Since in most of the cases we cannot avoid tracking people and goods, for all the encouraging reasons outlined above, a compromise should be found. A possible outcome could be to encrypt navigation solution, exploiting innovative technological solutions, in order to limit the amount of position information handed out. Instead of live tracking the speed of a vehicle, the employer's could only be able to see whether it exceeds the limits. Alternative scenarios are then represented by stricter and clearer rules and regulations.

8.4 Conclusions

The increasing popularity of GNSS-based tracking underlines the importance of dealing with ethical aspects in the future. Several major implications have arisen from the few situations analysed, which are relevant to the stakeholders network, in particular in the case of people who impose tracking on others.

The use of GPS tracking systems is mainly based on care, control and convenience. The different balance between these three aspects in different situations leads to ethical issues.

Clearly, tracking makes life much easier: governments can use GPS trackers on parolees and sex offenders to reduce the cost of detainment. Employers can track their workers to maximise profit by ensuring they are working. Parents track their kids because they are too busy to watch over them. Additionally, tracking dementia sufferers is essential because the number of aged carers is too few and the need is too great. GNSS can potentially save lives. Despite these facts, in some cases it is used for the wrong reasons or misused by some individuals and groups. Tracking is very invasive so care must be taken to ensure that only **essential information** about that person is revealed. Furthermore, the problem of GNSS jamming and spoofing has to be considered, since it introduces more complex ethical questions. Technological convergence and regulations are finally needed to correct the majority of these issues

Conclusions

The thesis deals with snapshot estimation techniques for GNSS mass-market receivers. The main objective of the work was to study, develop and demonstrate the main estimation algorithms currently used in consumer devices, by focusing mainly on the porting of the techniques in a SDR platform, on the innovation of state-of-the-art methods, on the adaptation of such techniques to the Galileo OS signal structure and on performance assessment and comparison.

As an introduction, Chapter 1 gives a brief and general overview on navigation technologies and on GNSSs fundamentals. The signal and system model is then presented in Chapter 2, with a particular focus on GPS L1 C/A and Galileo OS E1BC signals, which are then considered in the development of the work.

In Chapter 3 the strategic role of mass-market navigation receivers is outlined. It has been shown as the receivers market share is dominated by consumer devices, and the trend for the following years is evident. Furthermore, receivers manufacturers are pushing towards multi-constellation solutions, able to improve performance, robustness, TTFF and power consumption. The architectural difference between standard and mass-market receivers architecture is presented. It is shown that snapshot estimation techniques are based on a multi-correlator open-loop structure, rather than on the classical dual-step acquisition and tracking closed-loop structure. In particular, this architecture enables the employ of snapshot estimation techniques, analysed in the thesis. Then, the main drivers leading the design of a commercial device are identified: the TTFF, the sensitivity and the power consumption. In the development of the thesis a section is dedicated to each of them, providing further analyses and results. At the same time, the concept of AGNSS is introduced; it is proved that AGNSS and snapshot estimation techniques undergo the same principle concerning code delay and Doppler frequency search space. To conclude this part, the scenarios used in the simulations are described.

The state-of-the-art description, the theoretical analysis development and the improvements related to snapshot estimation are reported in Chapter 4. At the same time, Chapter 5 presents some results related to each technique proposed. What is more, in order to assess the technique possibilities and performance, a fully software receiver running on a PC has been implemented; it represents a very flexible and powerful research tool. The theoretical concepts behind the multi-correlation open-loop snapshot processing structure have been proposed and deeply investigated. The open-loop paradigm has been presented and described. Then three different parameters estimation options have been outlined; among them, the reduced search space, representing the fundamental element of snapshot estimation algorithms, has been considered throughout the work. Code delay and Doppler frequency estimation techniques have been described and deeply investigated. Results proved that they reach at least the same performance of their equivalent closed-loop DLL and PLL implementation, maintaining the benefits of the open-loop approach. Also the problem of search space windowing, that is the transition from one reduced search space to another, has been addressed, both from the theoretical and experimental point of view. Among all the methods proposed, an innovative frequency estimation technique based on FFT has been deeply investigated. A complete mathematical background has been provided; extensive simulation campaigns have

been performed and finally results in terms of estimate performance have been given, outlining the excellent capabilities of this algorithm, which outperforms any other snapshot-based frequency estimation technique. Power saving on demand processing, in the particular case of duty cycle processing, has then been introduced, as a particular application of snapshot estimation techniques. It has been shown that it is possible to periodically switch off the receiver to save computational power, almost without compromising the estimate accuracy. To conclude and provide a further confirmation of the goodness of such techniques, real Galileo IOV signals have been processed with the fully software receiver implemented exploiting the techniques proposed. In parallel to the design, the development and the implementation of mass-market algorithm in the software receiver, some tests have been performed exploiting a real Galileo ready mass-market receiver evaluation board; results in terms of TTFF, GGTO and sensitivity have been presented.

The results are extremely interesting and promising, and confirm the importance of snapshot estimation techniques and architecture in the frame of GNSS receivers, also for multi-constellation environments and in the particular case of SDRs. The reduced search space has been shown to be an excellent compromise between the traditional full search space typical of acquisition and the local search space of traditional tracking loops. It has been proved by means of semi-analytical simulations that the code delay estimation error is almost identical to the theoretical DLL tracking jitter, at least for signals with $C/N_0 > 35$ dBHz. At the same time it has been shown that the Doppler frequency estimation error, when exploiting the advanced FFT technique, is as good as the CRLB for signals with $C/N_0 > 30$ dBHz. Results can improve when increasing to nominal size of the snapshot (64 ms). The windowing process capabilities have been confirmed, also in the case of on demand duty cycle processing. Finally, the PVT solution obtained with both hardware simulated and real data confirms the capabilities of the whole system.

For sake of completeness, a brief overview on carrier phase estimation is provided in Chapter 6. It is expected, in fact, that in the near future carrier phase measurements will be considered also for single frequency mass-market receivers. This will dramatically improve the performance. However, several problems still need to be faced, such as the detection and mitigation of cycle slips. It has been shown that, at present, technology is not enough mature for implementing carrier phase positioning on a consumer device.

Summarizing, this thesis presents a complete and innovative overview and implementation solution of snapshot-based open-loop estimation techniques. Tests, simulations and comparisons support the potentialities of such algorithms for software receivers implementations tailoring the consumer market.

Future activities

Future activities and suggested works on the topic include the transparent integration with AGNSS technology and the development of a standalone fully software receiver. What is more, a deep investigation of carrier phase positioning can lead to the introduction of such measures in mass-market receivers, thus entering a new era for GNSS receivers technology.

Appendices

Appendix A

Software and Hardware Tools Description

Several different hardware and software tools were used during the work. A short description is provided hereafter.

A.1 N-FUELS

N-FUELS is a MATLAB™-based GNSS signal generator and analyser that allows the simulation of physical layer signal structure for GPS, Galileo and EGNOS systems in all the current and future bands (L1, L2 and L5 for GPS, E1, E5 and E6 for Galileo), as seen at the front-end output of a digital receiver, right after ADC, either at IF or at baseband. It has been developed by the researchers of the NavSAS group of ISMB and Politecnico di Torino.

The signal generator has a Graphical User Interface (GUI) (Figure A.1), allowing the user to change a variety of parameters. The signal samples are possibly impaired by noise, multipath, Doppler effect, interferences of different nature (i.e. intra-system, intersystem, bandlimited, continuous wave), AWGN, receiver front-end characteristics (equivalent receive filter, ADC), and can carry the navigation message read from an ad-hoc file.

Thereby, a reliable, though non real time, simulation of the received signal samples after ADC conversion is made available at a sampling frequency, quantization and format open to the user's setting. This signal, usually denoted raw signal, is a binary file containing raw GNSS samples, and is usually processed with a SDR GNSS receiver for different research purposes. This allows the test of any reception algorithm that processes digital samples in a completely controlled signal/environmental scenario, e.g. acquisition algorithms, code and carriers tracking loops, C/N_0 estimation algorithms, interference or multipath detection and mitigation algorithms and so on.

A conceptual scheme of the elements included in the signal generator is sketched in Figure A.2, where:

- **SIS** indicates the generation of the SIS for one or more satellites;
- **DISTURBANCES** indicates the generation of the disturbing signals (e.g., interference or multipath);
- **NOISE** indicates the generation of the AWGN.

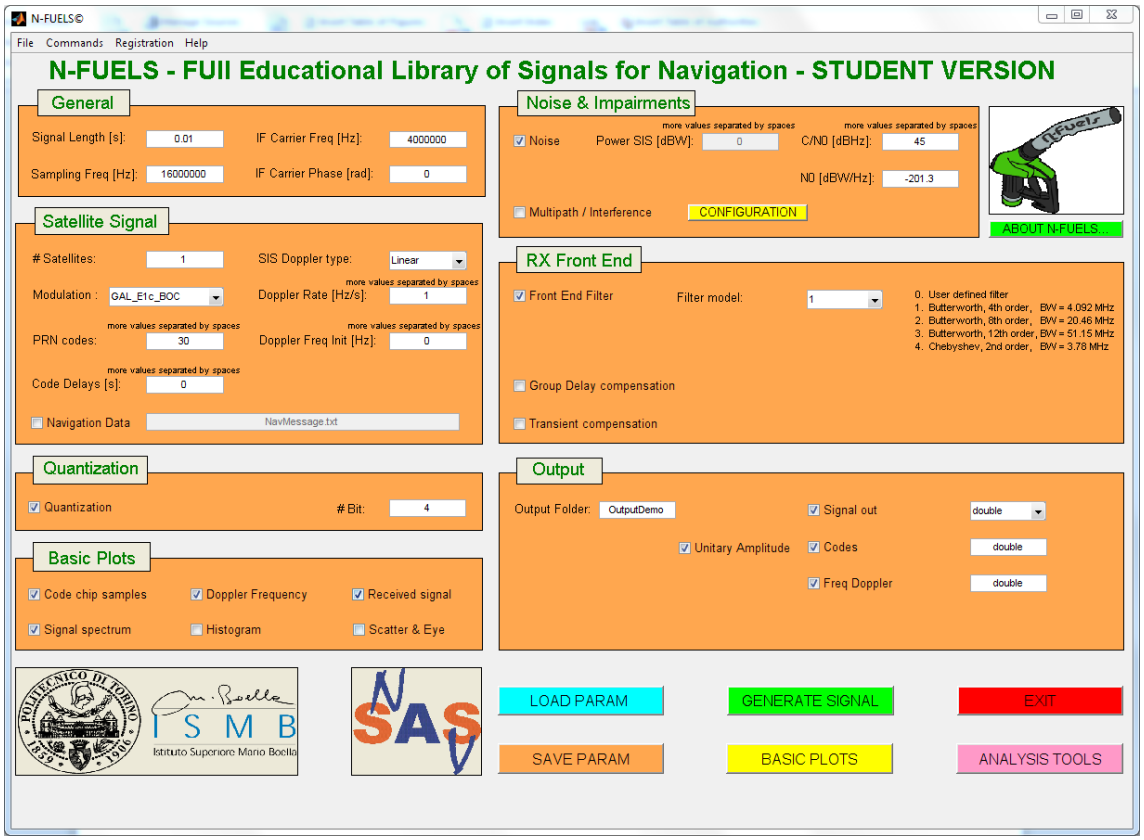

Figure A.1: N-FUELS student version screenshot.

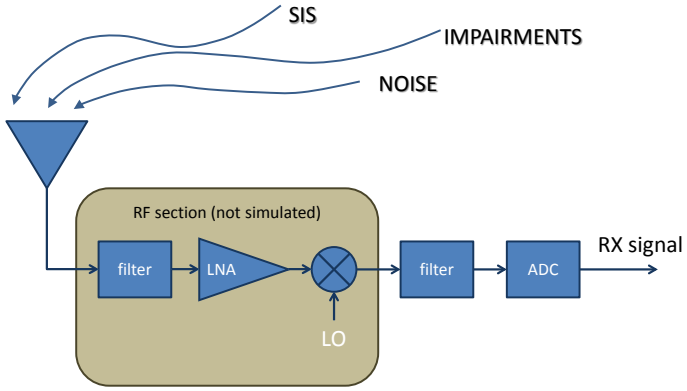

Figure A.2: Structure of the N-FUELS signal generator.

For these reasons, the tool represents an appealing, low-cost, quick, powerful and almost essential tool for conducting research in the navigation field, in order to test new algorithm, evaluate their performance and compare results.

A.1.1 A cloud GNSS signal generator

According to a survey, the main problems to face when using N-FUELS are the following:

- **Execution time**: the generation of a standard data set, consisting of 10 Galileo E1BC signals for a total length of 1 minute, takes about 4 hours on a standard personal computer. Using more complicated modulations and adding propagation effects, such as interference or multipath, can further increase the execution time.

- **Resource demand**: the software is very demanding in terms of RAM. When using N-FUELS on a standard pc any other process has limited resources available.

- **Size** of the output data: depending on the sampling frequency and on the file format, the data set can reach important dimensions, up to a few gigabytes.

- **License** and availability of the last version: the software is updated very often; moreover it is distributed with a license key. Therefore, at each update, it is necessary to distribute it to the user and to repeat the registration process.

It is interesting to point out that all these problems can be easily and cleverly solved exploiting **cloud computing**.

A.1.2 Adding cloud capabilities to N-FUELS

In order to solve the problems outlined above it is possible to move to a cloud infrastructure. In fact, one of the main benefits of the cloud technology is to have a more powerful machine available, and then to reduce the simulation execution time. In addition, the resources allocation in a cloud infrastructure is controlled by a hyper-visor; therefore, more RAM can be given to some user when necessary, in order to complete a simulation.

Furthermore, by creating a virtualized and collaborative environment, the cost of the Information and Communication Technology (ICT) infrastructure is reduced: instead of having 15 machines running N-FUELS, only one powerful shared machine is present. In this particular case, the paradigm of Platform As A Service (PAAS) can be exploited. The user just needs the control on the application at the operating system level, as well as the access to the hard drive in order to copy the data. In a future development, by modifying the N-FUELS user interface, it is possible to move to the Software As A Service (SAAS) solution.

Another advantage is represented by the storing and sharing possibilities. When more users need to access the same dataset, it is not necessary to rely on portable hard drives, but it is sufficient to access to a shared area on the cloud. Moreover, cloud computing offers a broad network access, ideal for using N-FUELS when out of the office, for example during a mission or a lecture. For security reasons, the private cloud is preferred. A good implementation solution could be the on site cloud development, exploiting the infrastructure already present at ISMB.

Finally, cloud computing technology offers a way to make N-FUELS more portable, interoperable and flexible. Only one instance of the program needs to be configured on the cloud, easing the updating process. In addition, only one license is then necessary, and the access can be controlled with a simpler mechanism of user-name and password. There is no longer the need to have a Microsoft Windows operating system and the Matlab Runtime Compiler (MRC) installed on every machine for each N-FUELS user. This represents a flexible and efficient use of the cloud computing technology, applied in the ICT field, enabling resources optimization, work simplification and cost reduction.

A.2 Front-end/bit-grabber

In order to test the different algorithms proposed with the software receiver described in Section 5.1, a file containing raw GNSS samples in a certain format is required. An hardware front-end, as described in Section 3.1.1, is then used to grab and store in a memory the signal samples. It has to be noted that the front-end is the only hardware component, along with the antenna, required by a SDR GNSS receiver to perform real data processing. The choice of the best front-end is usually a trade-off between the complexity of the different stages. The output of the front-end is a signal at IF that is usually processed by a data grabber, able to store the each sample of the digital GNSS stream in a memory, as binary data. A software receiver can then access to a file and process the signal in a proper way.

A.2.1 SiGE

SiGe GN3S Sampler front-ends are available at the NavSAS lab in ISMB. The SiGe GN3S Sampler is a high-end device, co-developed by the GNSS Lab at the University of Colorado and SiGe. It captures raw GNSS data to a binary file on a computer through Universal Serial Bus (USB) communication channel. An example is reported in Figure A.3.

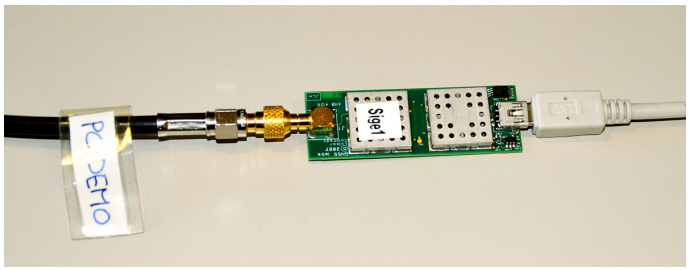

Figure A.3: Example of SiGE front-end/bit-grabber available at ISMB navigation lab.

A.2.2 MAX2769

The front-end/grabber used at ESTEC navigation lab is based on the Maxim/Dallas MAX2769 RF front-end. The MAX2769 is a GNSS front-ned covering GPS, GLONASS, and Galileo navigation satellite systems on a single chip (Maxim Integrated). This single-conversion, low-IF GNSS receiver is designed to provide high performance for a wide range of consumer applications. It incorporates on a chip the complete receiver chain, including a dual-input LNA and mixer, followed by the image-rejected filter, Voltage Controlled Oscillator (VCO), fractional-N frequency synthesizer, crystal oscillator, and a multi-bit ADC. The total cascaded noise figure of this receiver is as low as 1.4 dB. It has a user programmable IF frequency, configurable bandwidth of 2.5, 4.2, 8, or 18 MHz (18 MHz only in low-pass filter mode) and configurable sampling frequency of up to 40 MHz [104]. The baseband filter of the receiver can be programmed to be a low-pass filter or a complex bandpass filter. The low-pass filter can be configured as a 3rd-order Butterworth filter for a reduced group delay or a 5th-order Butterworth filter for a steeper out-of-band rejection. The two-sided 3 dB corner bandwidth can be selected to be 2.5 MHz, 4.2 MHz, 8 MHz, or 18 MHz.

A.3 Hardware signals generators

Hardware signal generators are simulation devices able to generate RF GNSS signals very similar to the true signals broadcast by the satellites and receiver on Earth. A generator can either be used directly connected to a receiver, such as the Teseo 2, or connected to a front-end and bit-grabber to store raw digital samples in a memory.

A.3.1 Spirent signal generator

A Spirent hardware signal generator was available at ESA ESTEC navigation lab. In particular L1 GPS C/A and E1 Galileo OS signals have been considered. Some particular features were exploited, such as the possibility to control the signal power by importing power files for generating LMS affected signals, or the configuration of the GGTO (Section 5.9.2).

A.3.2 NavX signal generator

A NavX® Navigation Constellation Simulator (NCS) hardware signal generator is present at ISMB Navigation lab. NavX is a single-frequency signal generator (GPS L1, Galileo E1, GLONASS G1, QZSS L1 and SBAS L1) and provides a maximum of 42 channels. It is controlled through a software running on a PC, providing full and easy access to all simulation parameters. A picture of the set-up is reported in Figure A.4.

Figure A.4: The NavX NCS hardware signal generator available at ISMB navigation lab.

A.4 Teseo 2 mass market evaluation board

A Teseo 2 evaluation board was available at ESA ESTEC navigation lab. A picture is reported in Figure A.5.

Figure A.5: The Teseo 2 evaluation board available at ESA ESTEC navigation lab.

Teseo 2 is a chip by STM, a stand-alone, single-chip positioning device capable of receiving signals from multiple satellite navigation systems, including GPS, Galileo, GLONASS and QZSS, and BeiDou in the future [105]. The Teseo 2 family combines high positioning accuracy and indoor sensitivity performance with powerful processing capabilities and superior design flexibility.

Teseo 2 is equipped with a Fastrax IT600 receiver module which provides the GNSS receiver functionality using the state of the art ST STA8088EX (System On Chip GNSS MCU Platform) chip. The Fastrax IT600 module is an advanced multi-constellation positioning and it has single RF input with separate GPS/Galileo and Glonass IF outputs combined with 32 dedicated tracking channels that can be assigned to acquire and track any mix of GPS, Glonass, QZSS Galileo and Compass signals. Unused tracking channels can be turned off for power saving.

Acronyms

ACF	Auto Correlation Function
ADC	Analog-to-Digital Converter
AGNSS	Assisted GNSS
A-GPS	Assisted GPS
APM	Advanced Power Management
ATP	Adaptive TricklePower™
AWGN	Additive White Gaussian Noise
BB	Base Band
BPSK	Binary Phase-Shifting Key
BOC	Binary Offset Carrier
C/A	Coarse Acquisition
CAF	Cross Ambiguity Function
CBOC	Composite Binary Offset Carrier
CDMA	Code Division Multiple Access
CET	Central European Time
C/N_0	Carrier-to-Noise density power ratio
CPU	Central Processing Unit
CRLB	Cramer-Rao Lower Bound
DC	Duty Cycle
DET	Department of Electronics and Telecommunications
DFFT	Double Fast Fourier Transform
DFT	Discrete Fourier Transform
DLL	Delay Lock Loop
DoD	Department of Defence

DSP	Digital Signal Processors
DSSS	Direct-Sequence Spread Spectrum
E	Early
EGNOS	European Geostationary Navigation Overlay System
ESA	European Space Agency
ESTEC	European Space Research and Technology Centre
FA	Full Active
FDMA	Frequency Division Multiple Access
FIR	Finite Impulse Response
FFT	Fast Fourier Transform
FLL	Frequency Lock Loop
FPGA	Field Programmable Gate Arrays
GA	Ground Antenna
GAGAN	GPS Aided Geo Augmented Navigation
GGTO	GPS Galileo Time Offset
GNSS	Global Navigation Satellite System
GPP	General Purpose Processor
GPS	Global Positioning System
GPST	GPS Time
GST	Galileo System Time
GTT	Gruppo Trasporti Torinese
GUI	Graphical User Interface
HDOP	Horizontal Dilution Of Precision
HOW	Handover Word
HDOP	Horizontal Dilution Of Precision
HS	High Sensitivity
I	In-phase
ICD	Interface Control Document
ICT	Information and Communication Technology
IF	Intermediate Frequency

IIF	Infinite Impulse Response
IOV	In-Orbit Validation
ISMB	Istituto Superiore Mario Boella
IRNSS	Indian Regional Navigational Satellite System
ISRO	Indian Space Research Organization
L	Late
LAN	Local Area Network
LBA	Location Based Application
LBS	Location Based Service
LMS	Land Mobile Satellite
LNA	Low Noise Amplifier
LOL	Loss of Lock
LOS	Line of Sight
LUT	Look-Up Table
MAT	Mean Acquisition Time
MCS	Master Control Station
MEO	Medium Earth Orbit
ML	Maximum Likelihood
MLE	Maximum Likelihood Estimator
MPM	Micro Power Management
MRC	Matlab Runtime Compiler
MS	Monitor Stations
MSAS	Multi-functional Satellite Augmentation System
NavSAS	Navigation, Signal Analysis and Simulation
NCO	Numerical Controlled Oscillator
NCS	Navigation Constellation Simulator
N-FUELS	Full Educational Library of Signals for Navigation
NMEA	National Marine Electronics Association
OS	Open Service
P	Precision

PAAS	Platform As A Service
PC	Personal Computer
PDA	Personal Digital Assistant
PLL	Phase Lock Loop
PDOP	Position Dilution Of Precision
PDP	Power Delay Profile
PFM	ProtoFlight Model
PND	Portable Navigation Device
PNT	Positioning, Navigation, and Timing
PRN	Pseudo-Random Noise
PPP	Precise Point Positioning
PTF	Push-To-Fix™
PVT	Position, Velocity and Time
Q	Quadrature
QZSS	Quasi-Zenith Satellite System
RF	Radio Frequency
RAM	Random Access Memory
RMS	Root Mean Square
RMSE	Root Mean Square Error
RTC	Real Time Clock
RTK	Real Time Kinematic
R&D	Research and Development
SIS	Signal-In-Space
SAAS	Software As A Service
SAR	Search And Rescue
SBAS	Satellite-Based Augmentation Service
SDR	Software Defined Radio
SNR	Signal-to-Noise Ratio
SoL	Safety of Life
SV	Space Vehicle

STM	ST Microelectronics
TAI	International Atomic Time
TCXO	Temperature Compensated Crystal Oscillator
TLM	Telemetry
TOA	Time Of Arrival
TP	TricklePower™
TTFF	Time To First Fix
UE	European Union
US	United States
USB	Universal Serial Bus
UTC	Universal Time Coordinates
VCO	Voltage Controlled Oscillator
WAAS	Wide Area Augmentation System
WAN	Wide Area Network
WGS84	World Geodetic System 1984

Bibliography

[1] E. S. Agency, "Birth of the European satellite navigation constellation," Luxembourg: Publication Office of the European Union, 2011.

[2] ——, "navipedia: The reference for global navigation satellite systems," http://www.navipedia.org/, January 2015.

[3] J. B. Y. Tsui, *Fundamentals of global positioning system receivers: a software approach*. Wiley-Interscience, 2005.

[4] P. Misra and P. Enge, *Global positioning system: signals, measurements and performance*. Massachusetts: Ganga-Jamuna Press, 2006.

[5] E. D. Kaplan and C. J. Hegarty, *Understanding GPS: principles and applications*. Artech house, 2006.

[6] M. Tahir, L. Lo Presti, and M. Fantino, "A novel quasi-open loop architecture for GNSS carrier recovery systems," *International Journal of Navigation and Observation*, pp. 1–12, 2012. [Online]. Available: http://www.hindawi.com/journals/ijno/2012/324858/

[7] National Coordination Office for Space-Based Positioning, Navigation, and Timing, "Official U.S. government information about the global positioning system (GPS) and related topics," http://www.gps.gov, January 2015.

[8] E. Commission, "EGNOS and GALILEO," Luxembourg: Publication Office of the European Union, 2012.

[9] European Global Navigation Satellite Systems Agency, "European GNSS service centre - constellation information," http://www.gsc-europa.eu/system-status/Constellation-Information, January 2015.

[10] P. G. Mattos and F. Pisoni, "Multi-constellation-to receive everything," in *Proceedings of the 25th International Technical Meeting of The Satellite Division of the Institute of Navigation (ION GNSS 2012)*, 2001, pp. 415–422.

[11] P. Mattos, "Adding GLONASS to the GPS/Galileo consumer receiver, with hooks for Compass," in *Proceedings of the 23rd International Technical Meeting of The Satellite Division of the Institute of Navigation (ION GNSS 2010)*, Sep 2010, pp. 2835–2839.

[12] Action team on Global Navigation Satellite Systems (GNSS), "GNSS follow-up to the third United Nations conference on the exploration and peaceful uses of outer space (UNISPACE III)," United nations, Tech. Rep. ST/SPACE/24, 2004.

[13] M. Shaw, "Presentation in torino," February 2008, presentation in Torino.

[14] D. Margaria, N. U. Linty, A. Favenza, M. Nicola, L. Musumeci, G. Falco, E. Falletti, M. Pini, M. Fantino, and F. Dovis, "Contact! - first acquisition and tracking of IOV Galileo signals," *INSIDE GNSS*, vol. 7, no. 1 - Ja, pp. 46–55, 2012.

[15] D. Margaria, M. Nicola, F. Dovis, N. Linty, and L. Musumeci, "Galileo in-orbit validation E1 and E5 signals: Experimental results and assessment," in *Proceedings of Satellite Navigation Technologies and European Workshop on GNSS Signals and Signal Processing (NAVITEC*

2012), 6th ESA Workshop on. Piscataway, NJ: IEEE - INST ELECTRICAL ELECTRONICS ENGINEERS INC, Dec 2012, pp. 1–8.

[16] M. Falcone, S. Binda, E. Breeuwer, J. Hahn, E. Spinelli, F. Gonzalez, G. López Risueño, P. Giordano, R. Swinden, G. Galluzzo, and A. Hedquist, "Galileo on its own first position fix," *Inside GNSS*, pp. 51–53, 2013.

[17] P. W. Ward, J. W. Betz, and C. J. Hegarty, "Satellite signal acquisition, tracking, and data demodulation," in *Understanding GPS: principles and applications*, A. House, Ed. Kaplan, E. and Hegarty, C., 2006, ch. 5, pp. 153–241.

[18] C. Chiasserini, "Ad hoc and sensor networks class notes," Gruppo reti, Politecnico di Torino, Tech. Rep., 2010.

[19] F. Dovis and P. Mulassano, *Introduction to Global Navigation Satellite Systems.* Unpublished, 2009.

[20] US Air Force, "Navstar GPS space segment/navigation user interfaces," 2004.

[21] Galileo Joint Undertaking, "Galileo open service signal in space interface control document (ICD)," 2010.

[22] G. Lachapelle, "Carrier phase positioning," PLAN group, Geomatics Engineering department, University of Calgary, Tech. Rep., 2013, presentations booklet of the ESA International Summerschool on GNSS 2013.

[23] G. Naden, "Global asset management, 11 years on," *GPS world*, 2015.

[24] M. O. Karaim, T. B. Karamat, A. Noureldin, M. Tamazin, and A. M. M., "Innovation: Cycle slips - detection and correction using inertial aiding," http://gpsworld.com/innovation-cycle-slips, January 2014.

[25] I. Mitola, Joseph, "Software radios: Survey, critical evaluation and future directions," *Aerospace and Electronic Systems Magazine, IEEE*, vol. 8, no. 4, pp. 25–36, April 1993.

[26] L. Lo Presti, E. Falletti, M. Nicola, and M. Troglia Gamba, "Software defined radio technology for GNSS receivers," in *Metrology for Aerospace (MetroAeroSpace), 2014 IEEE.* IEEE, May 2014, pp. 314–319.

[27] G. Povero, "GNSS introduction, link budget," Navigation Lab, ISMB, Tech. Rep., 2009, class notes of the Second Level Master in Navigation and Related Applications.

[28] D. Borio and C. O'Driscoll, "GNSS receiver design," PLAN group, Geomatics Engineering department, University of Calgary, Tech. Rep. ENGO 638, 2009.

[29] R. B. Langley, "GPS receiver system noise," *GPS world*, vol. 8, no. 6, pp. 40–45, 1997.

[30] F. Van Diggelen, "GPS and smartphones the technology revolution that put GPS in your phone," September 2009, plenary session presentation, 22nd International Meeting of the Satellite Division of The Institute of Navigation, Savannah, GA,.

[31] B. Parkinson, "Assured PNT for our future: PTA," *GPS world*, 2014, 25th Anniversary GNSS History Special Supplement.

[32] K. Borre, D. M. Akos, N. Bertelsen, P. Rinder, and S. H. Jensen, *A software-defined GPS and Galileo receiver: a single-frequency approach.* Springer, 2007.

[33] F. Van Graas, A. Soloviev, M. U. de Haag, and S. Gunawardena, "Closed-loop sequential signal processing and open-loop batch processing approaches for GNSS receiver design," *IEEE Journal of Selected Topics in Signal Processing*, vol. 3, no. 4, pp. 571–586, Aug 2009. [Online]. Available: http://ieeexplore.ieee.org/lpdocs/epic03/wrapper.htm?arnumber=5166586

[34] V. G. Rao and G. Lachapelle, "Will irnss solve the los ttff problem?" *Coordinates*, vol. 8, no. 12, 2012.

[35] C. Abraham, S. de la Porte, and S. Podshivalov, "Method and apparatus for performing signal correlation," USA Patent 7 190 712 B2, March 13, 2007.

[36] C. Abraham, E. Tapucu *et al.*, "Method and apparatus for performing signal correlation using historical correlation data," USA Patent 6 819 707 B2, July, 2009, US Patent 7,567,636.

[37] F. S. T. Van Diggelen, *A-GPS: assisted GPS, GNSS, and SBAS*. Artech House, 2009.

[38] N. Linty, L. Musumeci, and F. Dovis, "Assistance requirements definition for GNSS receivers in hostile environments," in *Proceedings of the 2014 International Conference on Localization and GNSS (ICL-GNSS 2014)*. Piscataway, NJ: IEEE - INST ELECTRICAL ELECTRONICS ENGINEERS INC, June 2014, pp. 1–6.

[39] N. Sokolova, D. Borio, B. Forssell, and G. Lachapelle, "Doppler rate measurements in standard and high sensitivity GPS receivers: Theoretical analysis and comparison," in *Indoor Positioning and Indoor Navigation (IPIN), 2010 International Conference on*. IEEE, Sep 2010, pp. 1–9.

[40] D. Arndt, T. Heyn, J. Konig, A. Ihlow, A. Heuberger, R. Prieto-Cerdeira, and E. Eberlein, "Extended two-state narrowband lms propagation model for S-band," in *Broadband Multimedia Systems and Broadcasting (BMSB), 2012 IEEE International Symposium on*, Jun 2012, pp. 1–6.

[41] F. Fontan, M. Vazquez-Castro, C. Cabado, J. Garcia, and E. Kubista, "Statistical modeling of the LMS channel," *Vehicular Technology, IEEE Transactions on*, vol. 50, no. 6, pp. 1549–1567, Nov 2001.

[42] Technical Specification Group Radio Access Network, "Evolved universal terrestrial radio access (E-UTRA); requirements for support of assisted global navigation satellite system (A-GNSS) (release 11)," 2012, 3rd Generation Partnership Project.

[43] J. G. Proakis and D. G. Manolakis, *Digital Signal Processing–Principles, Algorithms and Applications*. Prentice Hall, 1995.

[44] A. Broumandan and T. Lin, "Performance of GNSS time of arrival estimation techniques in multipath environments," in *Proceedings of the 21st International Technical Meeting of the Satellite Division of The Institute of Navigation (ION GNSS 2008)*, Sep 2008, pp. 632–643.

[45] N. Linty, "GNSS algorithms for mass-market positioning devices," European Space Agency, Tech. Rep., 2013, ESA Prestige programme 2012/2013, final report.

[46] N. F. Krasner, "Method for open loop tracking GPS signals," USA Patent 0 084 933 A1, October, 2003, uS Patent 6,633,255.

[47] Z. Jia and C.-S. Wang, "Fast Fourier transform with down sampling based navigational satellite signal tracking," USA Patent 0 046 536 A1, August 31, 2005, uS Patent 11/218,298.

[48] C. E. Shannon, "Communication in the presence of noise," *Proceedings of the IRE*, vol. 37, no. 1, pp. 10–21, Jan 1949.

[49] X. Tang, E. Falletti, and L. Lo Presti, "Fast nearly ML estimation of Doppler frequency in GNSS signal acquisition process," *Sensors*, vol. 13, no. 5, pp. 5649–5670, Apr 2013. [Online]. Available: http://www.mdpi.com/1424-8220/13/5/5649/

[50] M. Karan, R. C. Williamson, and B. D. O. Anderson, "Performance of the maximum likelihood constant frequency estimator for frequency tracking," *IEEE Transactions on Signal Processing*, vol. 42, no. 10, pp. 2749–2757, 1994. [Online]. Available: http://ieeexplore.ieee.org/lpdocs/epic03/wrapper.htm?arnumber=324740

[51] E. Jacobsen and P. Kootsookos, "Fast, accurate frequency estimators (DSP tips & tricks)," *IEEE Signal Processing Magazine*, vol. 24, no. 3, pp. 123–125, May 2007. [Online]. Available: http://ieeexplore.ieee.org/lpdocs/epic03/wrapper.htm?arnumber=4205098

[52] Y. Liao, "Phase and frequency estimation: High-accuracy and low-complexity techniques," Ph.D. dissertation, Worcester Polytechnic Institute, 2011.

[53] M. Petovello, "Markets and multi-frequency GNSS," *INSIDE GNSS*, vol. 1, pp. 34–37, 2013.

[54] M. A. Richards, "The discrete-time Fourier transform and discrete Fourier transform of windowed stationary white noise," Georgia Institute of Technology, Tech. Rep., 2007.

[55] N. Linty, L. Presti, F. Dovis, and P. Crosta, "Performance analysis of duty-cycle power saving techniques in GNSS mass-market receivers," in *Position, Location and Navigation Symposium*

- *PLANS 2014 IEEE/ION*. Monterey, CA: Institute of Electrical and Electronics Engineers Inc., May 2014, pp. 1096–1104.

[56] N. Linty and P. Crosta, "Code and frequency estimation in Galileo mass market receivers," in *Proceedings of the 2013 International Conference on Localization and GNSS (ICL-GNSS 2013)*. Piscataway, NJ: IEEE - INST ELECTRICAL ELECTRONICS ENGINEERS INC, June 2013, pp. 1–6.

[57] Z. Zhuang, K.-H. Kim, and J. P. Singh, "Improving energy efficiency of location sensing on smartphones," in *Proceedings of the 8th International Conference on Mobile Systems, Applications, and Services*. New York, NY, USA: ACM, 2010, pp. 315–330. [Online]. Available: http://doi.acm.org/10.1145/1814433.1814464

[58] I. Zahid, M. A. Ali, and R. Nassr, "Android smartphone: Battery saving service," in *Research and Innovation in Information Systems (ICRIIS), 2011 International Conference on*. IEEE, Nov 2011, pp. 1–4.

[59] D. Raskovic and D. Giessel, "Battery-aware embedded GPS receiver node," in *Mobile and Ubiquitous Systems: Networking & Services, 2007. MobiQuitous 2007. Fourth Annual International Conference on*. IEEE, Aug 2007, pp. 1–6.

[60] J. Kwak, J. Kim, and S. Chong, "Energy-optimal collaborative GPS localization with short range communication," in *Modeling & Optimization in Mobile, Ad Hoc & Wireless Networks (WiOpt), 2013 11th International Symposium on*. IEEE, May 2013, pp. 256–263.

[61] Z. Jia, S. A. Kurethaya, and C.-S. Wang, "Navigational signal tracking in low power mode," USA Patent 7 847 726 B2, December, 2010, uS Patent 7,847,726.

[62] L. Young and A. Reza, "SiRF application note power management considerations of SiRFstarIII," SiRF Technology, Inc., Tech. Rep., 2005.

[63] Telit, "JF2/JN3 low power modes," Telit Communications S.p.A, Application Note 80000NT10062A Rev.5, 2012.

[64] N. Linty and P. Crosta, "Galileo/GPS mass market receivers: Tracking algorithms analysis and performance," in *Proceedings of the 31st AIAA International Communications Satellite Systems Conference (ICSSC 2013)*. Lawrenceville: FGM EVENTS LLC, 2013, pp. 1–14.

[65] D. Borio, L. Camoriano, and L. Lo Presti, "Impact of GPS acquisition strategy on decision probabilities," *Aerospace and Electronic Systems, IEEE Transactions on*, vol. 44, no. 3, pp. 996–1011, July 2008.

[66] K. Ali, E. G. Manfredini, and F. Dovis, "Vestigial signal defense hrough signal quality monitoring techniques based on joint use of two metrics," in *Position, Location and Navigation Symposium-PLANS 2014, 2014 IEEE/ION*. IEEE, May 2014, pp. 1240–1247.

[67] L. Musumeci and F. Dovis, "Use of the wavelet transform for interference detection and mitigation in global navigation satellite systems," *International Journal of Navigation and Observation*, vol. 2014, 2014.

[68] 3GPP TS, "Technical specification group radio access network; evolved universal terrestrial radio access (E-UTRA); requirements for support of assisted global navigation satellite system (A-GNSS)," 3rd Generation Partnership Project, Tech. Rep. Release 11, 2012.

[69] S. Lannelongue and P. Pablos, "Fast acquisition techniques for GPS receivers," in *Proceedings of the 54th Annual Meeting of The Institute of Navigation*, 1998, pp. 261–269.

[70] W. J. Hurd, J. I. Statman, and V. A. Vilnrotter, "High dynamic GPS receiver using maximum likelihood estimation and frequency tracking," *IEEE Transactions on Aerospace and Electronic Systems*, vol. AES-23, no. 4, pp. 425–437, Jul 1987. [Online]. Available: http://ieeexplore.ieee.org/lpdocs/epic03/wrapper.htm?arnumber=4104371

[71] V. Clarkson, "Efficient single frequency estimators," in *Proceedings of the International Symposium on Signal Processing andApplications*. Gold Coast: Citeseer, 1992.

[72] N. Linty, P. Crosta, P. G. Mattos, and F. Pisoni, "An insight on mass market receivers algorithms and their performance with Galileo OS," in *Proceedings of the 26th International*

Technical Meeting of The Satellite Division of the Institute of Navigation (ION GNSS 2013). Manassas, VA (USA): Institute of Navigation, Sep 2013, pp. 2852–2861.

[73] European Global Navigation Satellite Systems Agency, "European GNSS service centre - constellation information," http://www.gsc-europa.eu/system-status/Constellation-Information, June 2014.

[74] M. Paonni, M. Anghileri, S. Wallner, J.-A. Avila-Rodriguez, and B. Eissfeller, "Performance assessment of GNSS signals in terms of time to first fix for cold, warm and hot start," in *Proceedings of the 2010 International Technical Meeting of The Institute of Navigation*, Jan 2001, pp. 1051–1066.

[75] I. Vanschoenbeek, B. Bonhoure, M. Boschetti, and J. Legenne, "GNSS time offset: Effects on GPS-Galileo interoperability performance," *Inside GNSS*, vol. 2, no. 6, pp. 60–70, 2007.

[76] A. Moudrak, A. Konovaltsev, J. Furthner, J. Hammesfahr, A. Bauch, P. Defraigne, and S. Bedrich, "Timing aspects of gps-galileo interoperability: challenges and solutions," DTIC Document, Tech. Rep., 2004, annual Precise Time and Time Interval (PTTI) Systems and Applications Meeting.

[77] J. H. Hahn and E. D. Powers, "Implementation of the GPS to Galileo time offset (GGTO)," in *Frequency Control Symposium and Exposition, 2005. Proceedings of the 2005 IEEE International*. IEEE, Aug 2005, pp. 33–37.

[78] E. Falletti, "Carrier phase positioning," Navigation Lab, ISMB, Tech. Rep., 2012, class notes of the Second Level Master in Navigation and Related Applications.

[79] M. O. Karaim, "Real-time cycle-slip detection and correction for land vehicle navigation using inertial aiding," Ph.D. dissertation, Queen's University, Kingston, Ontario, Canada, 2013.

[80] H. Meyr, M. Moeneclaey, and S. Fechtel, *Digital Communication Receivers: Synchronization, Channel Estimation, and Signal Processing*. New York, NY, USA: John Wiley & Sons, Inc., 1997.

[81] M. Kirkko-Jaakkola, J. Traugott, D. Odijk, J. Collin, G. Sachs, and F. Holzapfel, "A RAIM approach to GNSS outlier and cycle slip detection using L1 carrier phase time-differences," in *Signal Processing Systems, 2009. SiPS 2009. IEEE Workshop on*. IEEE, 2009, pp. 273–278.

[82] Z. Ren, L. Li, J. Zhong, M. Zhao, and Y. Shen, "A real-time cycle-slip detection and repair method for single frequency GPS receiver," *International Proceedings of Computer Science and Information Technology (IPCSIT)*, vol. 17, pp. 224–230, 2011.

[83] H. Hu and L. Fang, "GPS cycle slip detection and correction based on high order difference and Lagrange interpolation," in *Power Electronics and Intelligent Transportation System (PEITS), 2009 2nd International Conference on*, vol. 1, Dec 2009, pp. 384–387.

[84] L. Ting, L. Suilao, W. Rui, J. Wei, and J. Jichao, "Adaptive detection and modification algorithm of gps cycle slips based on wavelet analysis," in *Mechatronic Science, Electric Engineering and Computer (MEC), 2011 International Conference on*, Aug 2011, pp. 1907 – 1910.

[85] T. Yi, H. Li, and G. Wang, "Cycle slip detection and correction of GPS carrier phase based on wavelet transform and neural network," in *Intelligent Systems Design and Applications, 2006. ISDA '06. Sixth International Conference on*, vol. 1, Oct 2006, pp. 46–50.

[86] B. Hofmann-Wellenhof, H. Lichtenegger, and J. Collins, *GPS Theory and Practice*, 5th ed. Wien (Austria): Springer, 1993.

[87] S. B. Bisnath, D. Kim, and R. B. Langley, "Carrier phase slips: a new approach to an old problem," *GPS World*, vol. 12, no. 5, pp. 2–7, 2001.

[88] Z. Dai, S. Knedlik, and O. Loffeld, "Cycle-slip detection, determination, and validation for triple-frequency GPS," in *Position, Location and Navigation Symposium, 2008 IEEE/ION*, May 2008, pp. 1060–1066.

[89] Z. Dai, "MATLAB software for GPS cycle-slip processing," *GPS Solutions*, vol. 16, no. 2, pp. 267–272, 2012.
[90] 5T srl, "Sito ufficiale 5T - Tecnologie Telematiche Trasporti Traffico Torino." http://www.5t.torino.it/.
[91] A. McNamee, "Ethical issues arising from the real time tracking and monitorining of people using GPS-based location services," Master's thesis, Faculty of Informatics, University of Wollongong, 2005.
[92] R. Landau and S. Werner, "Ethical aspects of using GPS for tracking people with dementia: recommendations for practice," *International Psychogeriatrics*, vol. 24, no. 3, p. 358, 2012.
[93] K. Michael, A. McNamee, and M. Michael, "The emerging ethics of humancentric GPS tracking and monitoring," in *Mobile Business, 2006. ICMB'06. International Conference on.* IEEE, June 2006, pp. 34–34.
[94] E. S. Agency, "Galileo services," http://www.esa.int/Our_Activities/Navigation/The_future_-_Galileo/Galileo_services, July 2010.
[95] "Ethics in computiong, study guide," http://ethics.csc.ncsu.edu/privacy/gps/study.php.
[96] J. E. Dobson and P. F. Fisher, "Geoslavery," *Technology and Society Magazine, IEEE*, vol. 22, no. 1, pp. 47–52, 2003.
[97] K. Sink, "Does GPS vehicle tracking equate to 'Big Brother?'," http://ezinearticles.com/?Does-GPS-Vehicle-Tracking-Equate-to-Big-Brother?&id=130897, January 2006.
[98] G. Kaupins and R. Minch, "Legal and ethical implications of employee location monitoring," in *System Sciences, 2005. HICSS'05. Proceedings of the 38th Annual Hawaii International Conference on.* IEEE, Jan 2005, pp. 133a–133a.
[99] A. Cameron, "GLONASS gone... then back," *GPS World*, April 2014.
[100] F. Dovis, L. Musumeci, N. Linty, and M. Pini, "Recent trends in interference mitigation and spoofing detection," *International Journal of Embedded and Real-Time Communication Systems (IJERTCS)*, vol. 3, no. 3, pp. 1–17, 2012.
[101] D. Loneghin, "Gli autisti Gtt: L'azienda ci spia con il GPS che controlla i bus," http://torino.repubblica.it/cronaca/2013/06/17/news/gli_autisto_gtt_l_azienda_ci_spia_con_il_gps_che_controlla_i_bus-61231576/, June 2013.
[102] A. Giambartolomei, "Torino, indagato l'ex amministratore di Gtt: "Spiati gli autisti degli autobus"," http://www.ilfattoquotidiano.it/2013/07/20/torino-indagato-lex-amministratore-di-gtt-spiati-autisti-degli-autobus/661879/, July 2013.
[103] D. Molnar and D. Wagner, "Privacy and security in library rfid: Issues, practices, and architectures," in *Proceedings of the 11th ACM Conference on Computer and Communications Security.* New York, NY, USA: ACM, 2004, pp. 210–219. [Online]. Available: http://doi.acm.org/10.1145/1030083.1030112
[104] F. Rodriguez, "Development of code and phase tracking algorithms for gnss signals in low c/n and high dynamics scenarios," Master's thesis, Università degli studi di Roma "La Sapzienza", 2011.
[105] STMicroelectronics, "GPS solutions - STMicroelectronics," http://www.st.com/internet/automotive/subclass/614.jsp, December 2012.